

SCUOLA DI SCIENZE

Dipartimento di Chimica Industriale “Toso Montanari”

Corso di Laurea Magistrale in

Chimica Industriale

Classe LM-71 - Scienze e Tecnologie della Chimica Industriale

**Synthesis, characterization and crystallization of
bionanocomposites based on PLLA, PCL and
nanocellulose.**

Tesi di laurea sperimentale

CANDIDATO

Alice Tavernelli

RELATORE

Chiar.mo Prof. Daniele Caretti

CORRELATORE

Prof. Alejandro J. Müller

Matteo Rizzuto

Sessione II

Anno Accademico 2014-2015

ABSTRACT

In recent years, environmental concerns and the expected shortage in the fossil reserves have increased further development of biomaterials. Among them, poly(lactide) PLA possess some potential properties such as good ability process, excellent tensile strength and stiffness equivalent to some commercial petroleum-based polymers (PP, PS, PET, etc.). This biobased polymer is also biodegradable and biocompatible However, one great disadvantage of commercial PLA is slow crystallization rate, which restricts its use in many fields.

Using of nanofillers is viewed as an efficient strategy to overcome this problem.

In this thesis, the effect of bionanofillers in neat PLA and in blends of poly (L-lactide)(PLA)/poly(ϵ -Caprolactone) (PCL) has been investigated. The used nanofillers are: poly(L-lactide-*co*- ϵ -caprolactone) and poly(L-lactide-*b*- ϵ -caprolactone) grafted on cellulose nanowhiskers and neat cellulose nanowhiskers (CNW). The grafting reaction of poly(L-lactide-*co*-caprolactone) and poly (L-lactide-*b*-caprolactone) on the nanocellulose has been performed by the *grafting from* technique. In this way the polymerization reaction it is directly initiated on the substrate surface. The condition of the reaction were chosen after a temperature and solvent screening.

By non-isothermal an isothermal DSC analysis the effect of bionanofillers on PLA and 80/20 PLA/PCL was evaluated.

Non-isothermal DSC scans show a nucleating effect of the bionanofillers on PLA. This effect is detectable during PLA crystallization from the glassy state. Cold crystallization temperature is reduced upon the addition of the poly(L-lactide-*b*-caprolactone) grafted on cellulose nanowhiskers that is most performing bionanofiller in acting as a nucleating agent.

On the other hand, DSC isothermal analysis on the overall crystallization rate indicate that cellulose nanowhiskers are best nucleating agents during isothermal crystallization from the melt state. In conclusion, nanofillers have different behavior depending on the processing conditions. However, the efficiency of our nanofillers as nucleating agent was clearly demonstrated in both isothermal as in non-isothermal condition.

Keywords: grafted random copolymers, grafted block copolymers, cellulose nanowhiskers, overall crystallization rate, isothermal crystallization rate, poly(L-lactide).

CONTENTS

ABBREVIATIONS USED IN THE THESIS.....	1
1. INTRODUCTION.....	2
1.1 Polyester.....	3
1.2 Poly(ϵ -caprolactone), PCL.....	4
1.3 Poly(lactic acid), PLA.....	5
1.4 PLA/PCL blend.....	8
1.5 Nanocellulose.....	10
1.6 Grafting to and from.....	12
1.7 Crystallization.....	14
1.8 Crystallization rate.....	15
1.8.1 Avrami theory.....	18
1.8.2 Lauritzen-Hoffman theory.....	19
2. OBJECTIVE OF THE THESIS.....	22
3. RESULTS AND DISCUSSION.....	23
3.1 Synthesis of CNW-g-P(LLA- <i>co</i> -CL) and CNW-g-P(LLA- <i>b</i> -CL) copolymers.....	23
3.2 Characterization of CNW-g-P(LLA- <i>co</i> -CL) and CNW-g-P(LLA- <i>b</i> -CL) copolymers.....	25
3.3 Preparation of the blends.....	35
3.4 Thermogravimetric analysis of blends.....	36
3.5 Differential scanning calorimetry (DSC): non-isothermal crystallization.....	40
3.6 Overall isothermal crystallization rate.....	47
4. CONCLUSIONS.....	63
5. EXPERIMENTAL SECTION.....	65
5.1 Materials.....	65
5.2 Synthesis in bulk of random co-polymer lactide and ϵ -caprolactone grafted on cellulose (CNW-g-P(LLA- <i>co</i> -CL)).....	65
5.3 Synthesis in bulk of random co-polymer lactide and ϵ -caprolactone grafted on cellulose (CNW-g-P(LLA- <i>co</i> -CL)).....	67
5.4 Synthesis in solution of block copolymer lactide and ϵ -caprolactone grafted on cellulose (CNW-g-P(LLA- <i>b</i> -CL)).....	67
5.5 Preparation of the blends.....	68
5.6 Product characterization.....	69
Reference:.....	71

ABBREVIATIONS USED IN THE THESIS

LA = racemic lactide

LLA = L-lactide isomer

CL = ϵ -caprolactone

PLA = poly(lactide)

PLLA = poly(L-lactide)

PDLA = poly(D-lactide)

PCL = poly (ϵ -caprolactone)

CNW = nanocellulose

CNW-g-P(LLA-*co*-CL) = Random copolymer poly(L-lactide-*co*- ϵ -caprolactone) grafted on nanocellulose

CNW-g-P(LLA-*b*-CL) = Block copolymer poly(L-lactide-*b*- ϵ -caprolactone) grafted on nanocellulose

DSC = Differential Scanning Calorimetry

TGA = Thermal Gravimetric Analysis

ATR-IR= Attenuated total reflection infrared spectroscopy

$^1\text{H-NMR}$ = Hydrogen-1 Nuclear Magnetic Resonance

T_m = melting temperature

T_m^0 = equilibrium melting temperature

T_c = crystallization temperature

ΔT = supercooling ($T_m^0 - T_c$)

1. INTRODUCTION

Polymers have an essential role in everyday life since they are robust, lightweight, inexpensive and chemically inert materials, although their disposal is considered a major problem regarding environmental impact. In recent years, there has been a change of route towards "biodegradable" bio-polymers, which are a large and interesting class of materials which can substitute in different applications traditional plastic with obvious environmental advantages. Biopolymers are classified according to the "*European Bioplastics Association*" as biodegradable polymers approved compostable according to EN 13432 that come from both renewable and non-renewable sources. Additionally, polymers from renewable sources can be either biodegradable or non-biodegradable.^[1]

Biodegradable polymers are divided into three categories depending on the source and the production process:

- Polymers directly extracted from biomass, such as polysaccharides, proteins and lipids.
- Polymers synthesized monomers from renewable biomass such as poly(lactic acid), or monomers from oil as poly(caprolactone).
- Polymer materials produced by microorganisms and genetically modified bacteria.^[2]

In the family of bio-polymers the poly(lactide) (PLA) it is currently one of the most promising materials on which both the academic and the industrial research is focusing, as clearly shown by the recent available literature, *reviews* and books.^[3-6]

PLA is considered to be biodegradable (suitable for short-term packaging) and biocompatible when in contact with living tissues (suitable for biomedical applications such as implants, sutures, capsules for medicines, etc.).

Typically, the thermodynamic, physical and mechanical properties of a semi-crystalline polymer, as PLA, depend on its structure and morphology.

Indeed, understanding the mechanism of crystallization, through the study of its rate, is the key to understand the behaviour of the polymer.

However, the major limit of commercial PLA is its slow crystallization rate, due to the presence of 1.2% of D-isomer in the material.

These limits are reflected in the slowing of the molding cycle.^[7, 8]

Using of nanocomposite is viewed as an efficient strategy to overcome the aforementioned drawback. Previous studies^[9] have highlighted how the cellulose nanowhiskers (CNW) increases PLA crystallization rate.

In order to ensure an effective transfer of nanofillers to a polymer matrix, it is essential to obtain a good interfacial adhesion as well as preventing their aggregation within the matrix. For this purpose, it is necessary to maximize the dispersibility of the CNW in the hydrophobic polymer matrix, as PLA and PCL, mitigating its hydrophilic characteristics by insertion on the cellulosic surface of relatively apolar organic functionalities.

One approach to overcome this problem is to modify the surface of the nanocellulose by grafting the polymer chains. The two most used approaches are called "*grafting from*" and "*grafting to*".^[9]

In the present case, "*the grafting from*" was preferred to "*the grafting to*", because a good degree of exfoliation and a high grafting density of nanocellulose are obtained. In literature, there are various methods to obtain the grafting on the surface of the nanocellulose; regarding the monomers studied here, the preferred option was a chain polymerization called surface-initiated ring-opening polymerization (SI-ROP).

We used the hydroxyl groups of the cellulose nanowhiskers as initiator, tin (II) 2-ethylhexanoate (Sn (Oct)₂) as catalyst for the polymerization of monomers such as ϵ -caprolactone (CL), L-lactide (LLA).^[9]

The aim of this thesis is to evaluate the change of the crystallization rate of PLA phase when the neat PLA and the PLA/PCL 80/20 blend are in presence of small amounts of nanofillers. The used nanofillers are: the poly (L-lactide-*co*-caprolactone) and poly (L-lactide-*b*-caprolactone) grafted on cellulose nanowhiskers, CNW-g-P(LLA-*co*-CL) and CNW-g-P(LLA-*b*-CL), and cellulose nanowhiskers, CNW. Through differential scanning calorimetry (DSC) and thermogravimetric (TGA) measurements, the different behaviours due to the different compositions of the copolymers have been studied. The overall crystallization rate (nucleation + growth) was investigated by isothermal DSC.

1.1 Polyester.

Linear aliphatic polyesters, being biocompatible and biodegradable, are the most important group of synthetic biodegradable polymers. Polyesters are biodegradable polymers due to the presence of labile ester linkages in the main chain: in practice, only the aliphatic polymers with methylene segments among the ester groups will degrade in a reasonable time, in fact PLA, degrades faster than PCL. Moreover, polyesters degrade hydrolytically through cleaving of the ester bond: this can be caused by enzymes or biological conditions or a combination of both. Polyesters which are derived from lactone and lactide can be

used in devices for controlled drug delivery and in biomedical applications since they are biocompatible. Unfortunately, the properties of the polyesters such as poly(lactic acid or lactide) (PLA) and poly(ϵ -caprolactone) are not adequate for the intended applications. However, the properties of these polymers can be improved through blend or copolymerization.

1.2 Poly(ϵ -caprolactone), PCL.

The poly(ϵ -caprolactone), or PCL, is a semi-crystalline polyester with a low glass transition temperature of about -60°C and a melting point of about 55°C .^[9] The amorphous component at room temperature is always rubber-like. This property is unusual among the most common aliphatic polyesters and contributes to the considerable permeability of PCL to many active principles. Thus, PCL is widely used in the design of devices for controlled release of drugs; an example is the CapronorTM, which is a system for the release of a contraceptive for a period of one year. Other important properties are its tendency to form compatible blends with many other polymers, and the possibility of obtaining copolymers with properties also significantly different from the original polymers. Although the PCL is synthesized from oil derivatives the presence of the ester linkage makes it a biodegradable material.

PCL is both biodegradable and biocompatible, PCL and its blends are used for a wide range of applications, such as in the packaging field, because it is easy to form even at a temperature of 60°C ; it is especially employed in the medical field.^[2]

The PCL is miscible with a large number of polymers such as polyvinyl chloride, polycarbonate and epoxy derivatives of bisphenol-A, while the majority of blends with other aliphatic polyesters are immiscible.

Generally, the PCL is polymerized starting from the ϵ -caprolactone (CL) monomer by Ring-Opening Polymerization (ROP), a process much studied in recent years.^[10]

ROP is based on the use of a one-, two-, multi-functional alcohol as initiator in the presence of a coordination complex (Sn, Zn, Al), typically originating from compounds such as Sn (ethylhexanoate)₂.

The polymerization starts normally from nucleophile species such as alcohol, both in the presence or absence of catalysts. The catalysts most used are organometallic compounds like tin or zinc derivatives, which react in situ with the alcohol, giving rise to alkoxides

which are responsible for the polymerization of the monomer according to a mechanism of coordination-insertion (see Figure 1.1) ^[11]

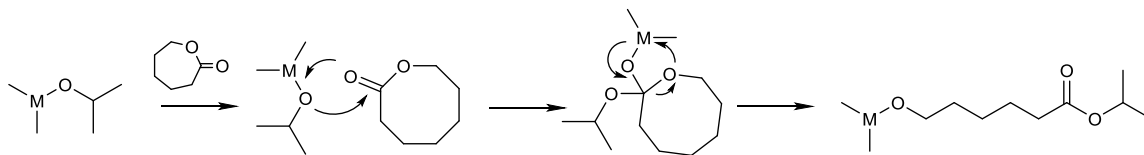


Figure 1.1 Mechanism of the initiation step for coordination–insertion ROP, adapted from Khanna et al. ^[12] and Stridsberg et al. ^[13]

1.3 Poly(lactic acid), PLA.

Polymers of poly(lactic acid), thanks to their good mechanical properties, high biocompatibility and biodegradability, are used in the medical field (suture material, prostheses, controlled release of drugs and support in the welding of fractured bone), in agriculture (plant containers and controlled release of nutrients) and packaging (coatings for packaging, bags and food containers). ^[9]

Lactic acid is generally industrially produced by the fermentation of carbohydrate starch from cereals such as corn, converting at 99.5% to the L(-) form and only at 0.5% to the D(+) form.

The synthesis of PLA from lactic acid can follow two ways: an indirect way through the lactide, which produces the "poly(lactide)", and one that provides direct polymerization through polycondensation, which gives the "poly(lactic acid)". The first way requires a pre-polymer of low molecular weight obtained by condensation of lactic acid in solution. The second method has been reported for the production of poly(lactic acid) by direct esterification of the molecules of lactic acid or by Ring Opening Polymerization (ROP), starting from a cyclic dimer of lactic acid, the 2,6-dimethyl-1,4-dioxan-2,5-dione (lactide). The process occurs through polycondensation, an equilibrium reaction. It is difficult to remove completely the water. Water limits the molecular weight due to hydrolysis of the ester bonds (as shown in figure 1.2). ^[14]

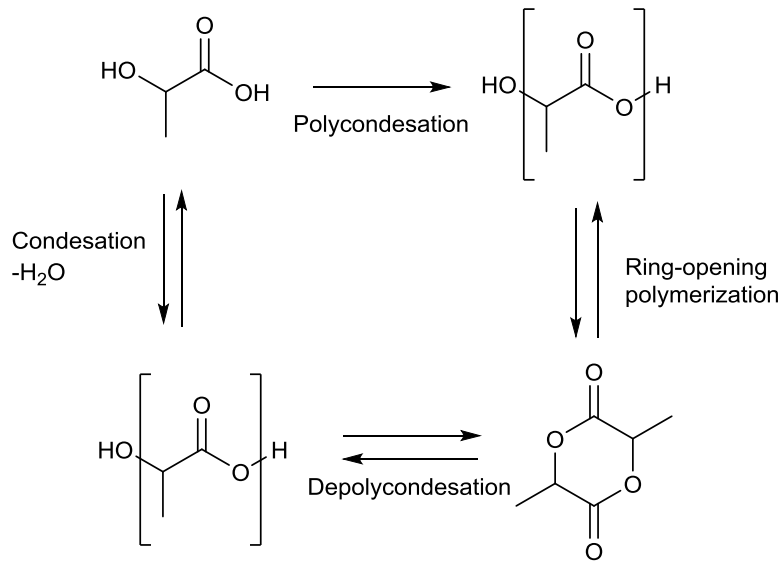


Figure 1.2 PLA production via prepolymer and lactide.

Many factors, such as molecular weight, degree of crystallinity, stereochemistry and the formulation of the material (the presence of plasticizers, other polymeric components in the blend, other components in composites, etc.), strongly influence the mechanical properties, which may vary the PLA behaviour from elastic to rigid. Taking into consideration the degree of crystallinity, amorphous polymers or less crystalline ones have lower elastic modules and a lower degree of stiffness, while crystalline polymers exhibit good mechanical properties. Then, the mechanical characteristics can be modified according to specific needs depending on the chosen formulation.

Lactic acid has three stereoisomeric forms which give three distinct polymers: PDLA, PLLA and PDLLA; the first two are the stereoregular (isotactic) semi-crystalline forms, while the latter, which is amorphous, is an atactic polymer constituted by units of D-lactic acid and L-lactic acid (as shown in figure 1.3).

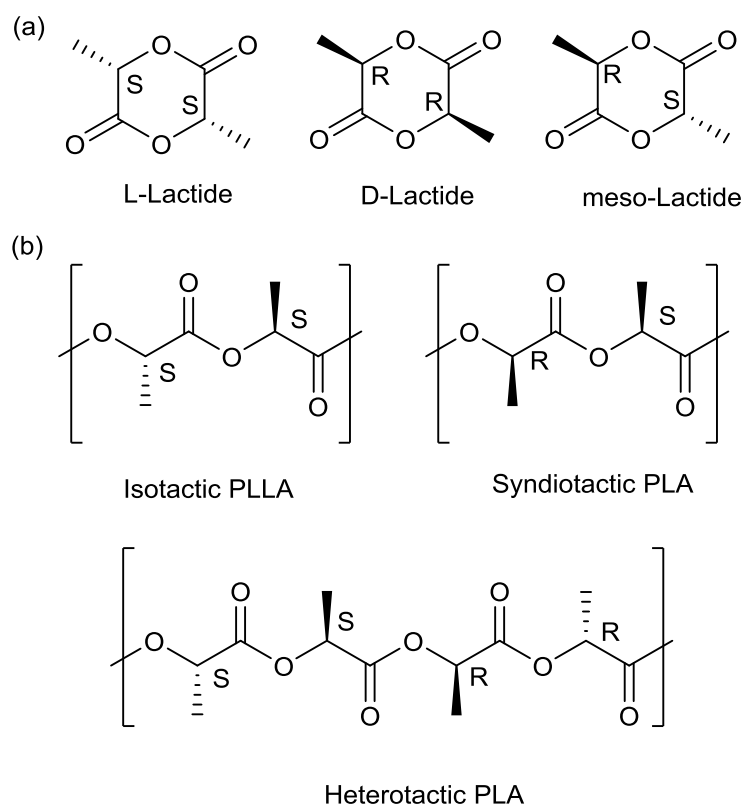


Figure 1.3 Stereochemistry of lactid acid and poly(lactide).^[15]

The ratio of D- and L-lactide determines the degree of crystallinity of the polymer: we can have either a totally amorphous PLA or a polymer with more than 40% of crystallinity. The degree of crystallinity influences several properties such as the tendency of the polymer to hydrolysis degradation. It has been demonstrated that a highly crystalline PLA requires months, if not years, to be completely degraded to lactic acid, while an amorphous polymer can be degraded in few weeks. This is due to the impermeability to water of the crystalline region.

The PLA obtained from L-lactide (PLLA) exhibits a melting temperature (T_m) between 170°C and 180°C: T_m can vary due to the presence of impurities and a certain, even minimal, racemization. In fact, both the D- and the meso-lactide introduce irregularities within the chain, causing a disorganization that limits the tendency to crystallize and prevents the formation of perfect crystals, thereby lowering the T_m .^[16]

Polymers with more than 93% of L-lactide are crystalline; polymers containing approximately 15% D-lactide and meso-lactide are amorphous. The glass transition temperature is situated between 50 and 80 °C. The rate of crystallization is quite slow, comparable to that of poly(ethylene terephthalate) (PET).^[1]

PLLA is preferably used in orthopaedic implants due to its good mechanical characteristics and toughness, thanks to its high crystallinity. PDLLA, being amorphous, is characterized by a kinetic of degradation faster than that of the semi-crystalline polymers (PLLA and PDLA), but its mechanical properties are poorer. Therefore, given these characteristics, PDLLA seems more suitable for applications in controlled drug release when a quick active substance release is required or, more generally, for implants that require a rather fast kinetics of biodegradation. ^[16]

PLA has low elasticity which can severely limit its use. Applying the blending techniques, mixed polymers were prepared with different characteristics than those of the first homopolymers. For example, PLA/PCL blends in which the presence of both monomers, in a variable ratio, and the control of the microstructure allow to modulate the properties of the copolymer in the final blend.

1.4 PLA/PCL blend.

A blend is a relatively simple and rapid approach in relation to the synthesis of the copolymers, and is of great interest for biomedical and environmental applications.

Blends can be created by either fusion or solution; the binary blends can be classified as amorphous/amorphous, semi-crystalline/amorphous and semi-crystalline/semi-crystalline. The blend with a semi-crystalline polymer and an amorphous one is the most used because it has higher impact resistance, toughness, ductility and further physical properties.

Blends can be miscible, semi-miscible and immiscible. The morphology of the immiscible blend is characterized by the presence of two phases. Two polymers, A and B, generally tend to form biphasic systems, considering that the increase of entropy associated with the mixing does not balance the unfavourable interactions between different chains. The formation of homogeneous mixtures depends on specific intermolecular interactions between different chains, on suitable molecular parameters (viscosity, molecular weight) and on the experimental conditions of blending. ^[17, 18]

Many commercial polymer blends are formed from immiscible components. They can be made more miscible ("compatible") through different experimental procedures, such as the addition of a compatibilizing agent. The compatibility between the components can also be improved by lowering the interfacial energy and reducing coalescence between phases; this has the effect of increasing the mechanical performance of the alloy and decreasing the average size of the areas of the dispersed phase.

The used compatibilizers are macromolecules that contain segments; sessions related to different homopolymers can promote molecular interactions (such as hydrogen bonds, covalent bonds, ionic interactions or chemical reactions between the components of the blend along the interface); these compounds thus reduce the surface tension at the interface and allow a greater dispersion and a greater adhesion between the phases. ^[19, 20]

Compatibilization may be divided into *ex situ*, which is the addition of a pre-synthetic copolymer, and *in-situ*, in which a copolymer is formed during the preparation of the blend. The mixing reagent is one of the more effective *in situ* techniques, as it generates directly the compatibilizing agent in the interface; however, blends consisting of more than two components are less studied due to their high complexity. The variables to be taken into consideration are the number of interphases to compatibilize, the viscosity of the components, the structure and chain length of all the components. The relative reactivity of the individual components during the reaction should also be considered, since in this process, in addition to the desired reaction (the formation of a compatibilizing agent), secondary processes can exist, such as chain scission and crosslinking. ^[21]

The *ex situ* compatibilization allows easier control of the molecular architecture compared to the previous method. In general, the most used pre-synthetic copolymers are block copolymers or grafted compatibilizers whose segments are chemically identical or have affinity with the components of the blend, of variable structure, capable of presenting themselves at the interface between the phases with an emulsifying action which promotes the dispersion of one phase in the other, and stabilizes the blend.

The PLA and PCL are immiscible, even if not highly incompatible ^[22]; therefore considerable efforts have been made in order to obtain a fine dispersion of the phases of mixed homopolymers, to create structures with good mechanical characteristics and obtain PCL domains with reduced dimensions, so as to increase the contact surface between the phases. Previous studies ^[9], have highlighted how copolymers CNW-g-P(CL-b-LA) diblock copolymers are able to perform an emulsifying action in the PCL and PLA/PCL blends.

Relying on these results, in this study the use of CNW-g-P(CL-b-LA) block copolymers and CNW-g-P(CL-co-LA) random copolymers has been experimented, even if the present work is mainly focused on the study of crystallization rate.

1.5 Nanocellulose.

Cellulose is the most common biopolymer in nature. It is produced from lignocellulosic biomass. The latter is composed by carbohydrate polymers (cellulose, hemicellulose) and aromatic polymers (lignin). The sources of most industrial materials used are agriculture waste (corn stover, bagasse from sugar cane, grass) and forestry (waste material from sawmills and paper production).

Cellulose is a homopolymer crystal in the form of long chains having high molecular weight, formed by the repetition of D-glucose units, which occurs widely in nature, linked together by β -1,4 glycosidic bond, as shown in figure 1.4. Each chain is characterized by the presence of a non-reducing end (in which the carbon C1 is involved in the glycosidic bond) and one reductant end (where C1 binds a hydroxyl group, thus allowing the opening of the glucose ring).

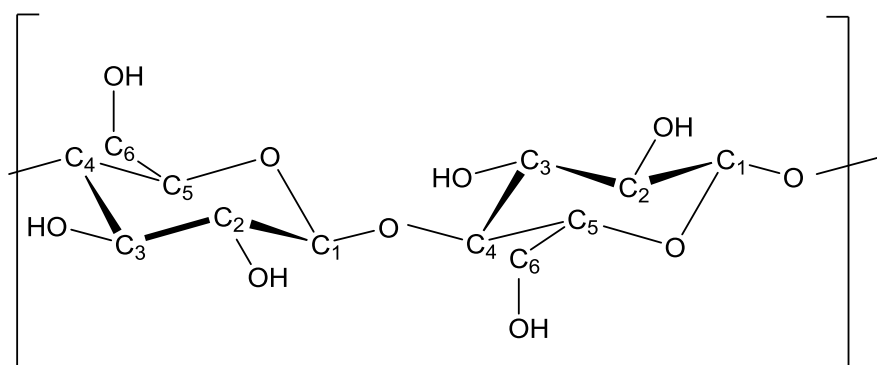


Figure 1.4 Molecular structure of a cellulose unit, showing the β 1-4 glucosidic bond and the intrachain hydrogen bonding. ^[23]

The three hydroxyl groups of each ring reside in the equatorial position along the average plane of the glycosidic unit, while the hydrogen atoms are in an axial position. The presence of the hydroxyl groups, in addition to providing hydrophilic characteristics to the polymer, is responsible for the formation of a complex network of intra- and inter-molecular hydrogen bonds that stabilize the single chain, allowing longer chains to aggregate thus forming the crystalline systems typically observed in cellulose fibres. Aggregation occurs thanks to Van der Waals forces and intra- and inter-molecular hydrogen bonds. ^[24]

The packing of the cellulose chains allows the creation of an ordered structure with high crystallinity; distributed randomly along the microfibrils there are para-crystalline or amorphous areas, which diminish the effectiveness of the internal forces. These amorphous

areas are at the origin of the formation process of the nanocrystalline cellulose: it exploits the selective hydrolysis of the glycosidic bonds of the amorphous areas, which, being less compact and with the highest energy, are more reactive than their crystalline counterparts. The cellulose nanowhiskers (CNW) is a type of nanocellulose obtained by acid hydrolysis of native cellulose. It differs from the bacterial cellulose (bacterial nanocellulose, BNC) and nanofibrillated cellulose (nanofibrillated/nanofibrillar cellulose, NFC) for its synthesis, morphology and its fields of application. The CNW, chemically produced, is in the form of thread-like crystalline structures (whiskers) with a diameter of about 5-70 nm and a length of a few hundred nanometers.^[25,26]

The nanocellulose properties is influenced by the following factors:

- temperature;
- reaction time;
- nature of the acid;
- acid-cellulose ratio.

The nature of the acid affects thermal stability. The most used acids are the sulphuric and hydrochloric acids.

If CNW's are prepared by the action of hydrochloric acid, their ability to de-aggregate is limited, and the colloidal dispersion generated in water tends to flocculate. When sulphuric acid is used as hydrolyzing agent, its reaction with the surface hydroxyl groups of the cellulose tends to yield negatively charged surface sulphate functionalities, enabling homogenous dispersions in water.

However, the introduction of charged sulphate groups compromises the thermostability of such nanocrystals, especially during nanocomposites processing, i.e. at elevated temperatures and in absence of solvents.^[25]

Different types of cellulose can be used in the synthesis of CNW, such as cotton, linen, hemp, pulp, bleached softwood and hard and microcrystalline cellulose.

Theoretically, the nanocellulose obtained by acid hydrolysis can be considered a material made of a single crystal cellulose (degree of crystallinity of 100%) since the hydrolysis removes the amorphous areas (microfibril defective areas). Actually, the hydrolysis is never complete and therefore the resulting product has a degree of crystallinity less than 100%.^[23]

The high rigidity of the nanocrystalline cellulose combined with the high tensile strength, high length-diameter ratio, high specific surface area and biodegradability^[27] make the CNW an excellent alternative to the inorganic fillers used in polymer materials. The

improvement of mechanical properties resulting from these fillers is given by the rigid "network" that the CNW makes due to the hydrogen bonds. The greater the adhesion between this network and the polymer matrix, the higher the improvement of the properties. For this purpose, it is necessary to maximize the dispersibility of the CNW in the hydrophobic polymer matrix, mitigating its hydrophilic characteristics by insertion on the cellulosic surface of a relatively apolar organic functionality.^[24]

In addition, CNW is readily available, renewable, and biodegradable.

CNW has a low thermal stability that limits its use, since the thermal decomposition temperature is in the range of 200-300 °C.

1.6 Grafting to and from.

As previously mentioned, nanocellulose is an excellent material for improving the application of bioplastics and biocomposites; however, cellulose in its native form is hydrophilic while the polymer matrices are usually hydrophobic, such as PLA and PCL, and this often leads to a low adhesion between the cellulose and the matrix.

One approach to overcome this problem is to modify the surface of the nanocellulose by grafting the polymer chains. The two most used approaches are called "grafting from" and "grafting to".^[28]

In the first approach, the monomers are directly polymerized from the surface in which the polymer chains are formed. The advantages of this technique are a good degree of exfoliation and a high grafting density; its major limitation is given by the fact that the surface of the cellulose has to be pre-treated to activate the polymerization.^[28] At industrial scale, this requires the use of organic solvents, making it more difficult to scale-up.

"Grafting to" binds the polymers acting at the surface of the cellulose and can be achieved in two ways: i) through a covalent bond by reacting one chain end of the polymer with functionalities on the cellulose surface; ii) noncovalently, utilizing electrostatic interactions. The covalent bond requires a highly versatile chemical approach and often involves a modification steps on the cellulose prior to the coupling, in order to introduce functional groups. The noncovalent coupling instead is based on the fact that negative charges can be easily incorporated into the cellulose structure. Consequently, cationically charged polyelectrolytes can be adsorbed onto the cellulose surface, under appropriate reaction conditions. One of the advantages in the use of this technique is the greater

molecular weight of the copolymer. It was concluded that the “grafting from” is superior to the “grafting to” in terms of the grafted polymeric amount on the surfaces.

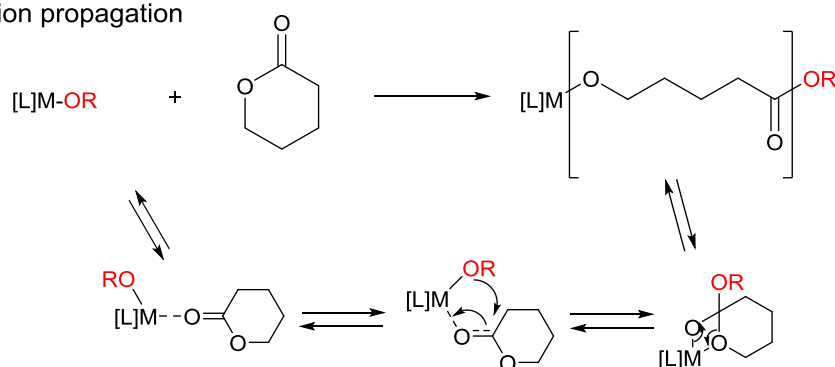
In the present case, “*the grafting from*” was preferred to “*the grafting to*”, since nanocellulose exfoliation is obtained. In literature, there are various methods to obtain the grafting on the surface of the nanocellulose; regarding the monomers studied here, the preferred option was a chain polymerization called surface-initiated ring-opening polymerisation (SI-ROP).

The hypothetical mechanism for the most accredited surface-initiated ring-opening polymerisation is coordination-insertion (as shown in figure 1.5).^[29] It is based on metal alkoxides having a covalent bond between oxygen and metal, with a weak Lewis acid behaviour. The lactide and caprolactone behave as a ligand that coordinates the metal atom with the oxygen bound to the carbonyl.^[30]

Active species generation



Initiation propagation



Exchange transfer reaction

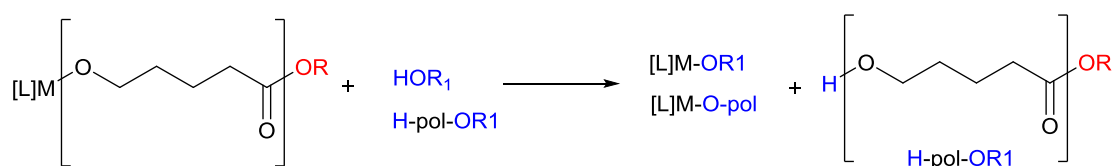


Figure 1.5 The proposed reaction pathway for the ROP of a cyclic ester by the coordination-insertion mechanism.^[29]

This improves the electrophilicity coordination of the carbonyl group (CO) and the nucleophilicity of the alkoxide group (OR), thus allowing the insertion of the lactide and caprolactone in the metal-oxygen bond. Typical initiators of this mechanism are alkoxides of magnesium, aluminium, tin, zirconium and zinc. Currently, the most widely used

compound is tin(II)octanoate (SnOct_2) due to its solubility properties, high catalytic activity and ability to promote the formation of polymers of high molecular weight with low level of racemization (<1%). In addition, tin(II)octanoate has a toxicity low enough to be tolerated by the US Food and Drug Administration (FDA). Alkoxides of tin(II) are not toxic, but during their degradation they can be converted in oxide or worse in the corresponding hydroxide, which is a strong base. ^[31]

We used the hydroxyl groups of the cellulose nanowhiskers as initiator, tin(II)-2-ethylhexanoate (Sn (Oct) 2) as catalyst for the polymerisation for monomers such as ϵ -caprolactone (CL), L-lactide (LLA).^[25]

1.7 Crystallization.

A material is solid in the crystal phase when their units are arranged in an orderly fashion according to a pattern repeated in space. One can thus identify a portion of a structure, the elementary cell, which contains all the operations of the crystal symmetry and which, shifted in the three directions of space, reproduces the crystal lattice.

In the case of polymeric materials, the chain must have particular characteristics in order to obtain a crystalline phase:

- Regular constitutional units (a polymer has a regular constitution if the repetition units are all equal to each other and have constant chaining)
- Regular configuration (regular polymer constitution or stereoregular whose linear molecules consist of monomeric units having either identical spatial configurations or configurations which, while not identical, alternate in regular fashion).
- Regularity of conformation (regular repetition of the structural elements along the axis of the chain and representable by means of a helix).

However, given the polymeric nature have very long chain which is composed of imperfections (such as irregularities in the chain, end groups, etc.), a polymer will never be completely crystalline, but will always have an amorphous part

The degree of crystallinity, the size of the crystals and molecular weight modify the physical and chemical properties of the material; therefore, in order to design a compound, it is very important to study its crystallization.

The fundamental unit of a crystalline is called a "lamella" and it occurs when different segments are arranged parallel to each other, helped by the regularity with which atoms

follow one another and therefore the ability to establish good intermolecular contacts. Chains are folded in the lamellae. When the crystallization takes place from the melt, the polymer superstructure arranges into spherulites.

The main feature of the spherulitic morphology are the lamellae which radiate in all directions from a central nucleus of crystallization, managing to homogeneously fill the whole spherical volume thanks to a mechanism of later branching. ^[32]

The opposite process of crystallization is the crystal melting which occurs when the polymer chain abandons its order in the crystalline structure and turns into a messy liquid. ^[33] The melting temperature (T_m) of the crystalline phase depends on molecular weight, on the thermal history and on the crystallization temperature (T_c). Crystallization is a process which occurs in a well-defined temperature range for each polymer.

The crystallization temperature is normally between 30°C above the glass transition temperature (T_g) and about 10°C below the melting temperature (T_m). ^[34] When the T_c is close to the T_m the macromolecular structure has a high mobility which facilitates the movement of the chains losing the ordered structure, and when the T_c is close to the T_g in this case we have a high viscosity and the chains have a lower mobility.

1.8 Crystallization rate.

The rate of crystallization is formed by two processes: the primary nucleation rate (I) and the crystalline growth rate (G).

Primary nucleation is the first step of crystallization. It can be heterogeneous or homogeneous.

Nucleation is homogeneous when it starts from the spontaneous aggregation of molecules or a segment of a chain due to thermal fluctuation in the heating, while heterogeneous nucleation requires a heterogeneity or nucleating agents inside the system; the second is the most common. ^[35] By adding nucleating agents, inside the molten mass of the polymer highly active heterogeneous nucleation areas are formed.

After the formation of primary nuclei follow a stage in which stable nuclei form on the surface of the growing crystal (secondary nucleation) and then develop.

The rate of growth occurs, instead, by means of a rearrangement of the crystalline phase already formed or a subsequent crystallization of polymer segments present in the amorphous phase, which entails an increase in the amount of crystalline material present in the sample.

The figure 1.6 shows the trend of the primary nucleation rate (I) and of the rate of crystal growth (G) with the temperature. Both have a bell-shaped trend, falling in the interval between T_g and T_m .

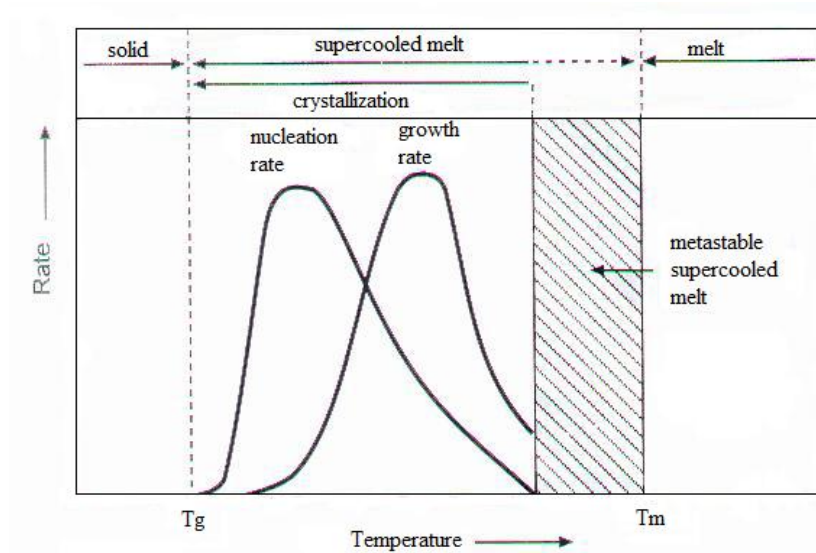


Figure 1.6 Temperature dependence of the nucleus formation rate and the crystallite growth rate on cooling from the melt. [9]

The trend of primary nucleation rate is highly dependent on many aspects such as; cooling and/or heating, thermal history, absence or presence of nucleating agents and other conditions.

On the other hand, the growth rate G only depends on the crystallization temperature and the molecular weight.

The overall rate of crystallization is given by the contribution of both rate (I) and (G); this function has a bell-shaped trend with a lower limit which depends on the glass transition temperature (T_g) of the material, and with the upper limit which depends on the melting temperature (T_m). The temperature of crystallization is very important since it determines the thermal energy of the macromolecules: at higher temperatures close to the melting point, the crystallization rate is very slow and the process is controlled by the nucleation because of the larger mobility of the polymer chains. On the other hand, lowering the temperature, the crystallization rate increases goes through a maximum and starts to decrease again when the crystallization is controlled by diffusion, which is hindered at low temperatures. The temperature parameter therefore has opposite effects on the rate of diffusion and deposition, and consequently on the overall crystallization rate, which will show a maximum at intermediate temperatures. (As shown in figure 1.7)

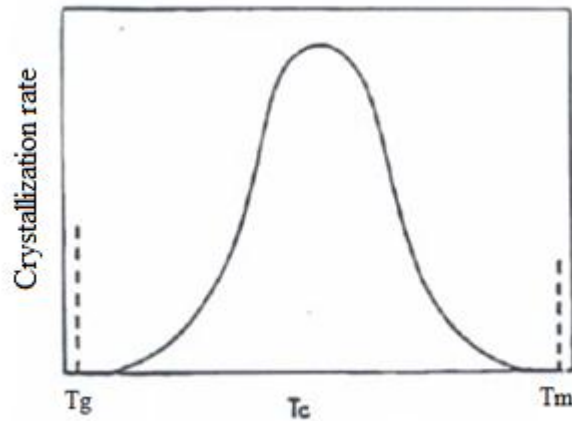


Figure 1.7 Crystallization rate vs. crystallization temperature.

Molecular weight has a significant role in the overall crystallization rate. Regarding molecular weight, also the overall crystallization has a bell-shaped trend, which depends on the performance of the processes of nucleation and accretion. The primary nucleation rate has an increasing trend with the increase of the weight molecules, while the growth rate has an opposite behaviour.

In the case of growth rate, if the polymer has a high molecular weight we have an increase of the crystallization temperature; inversely, chains of low molecular weight crystallize in a shorter time and at lower temperatures since high values of molecular weights slow down the diffusional processes. Instead, in the case of nucleation high molecular weight contributes to the stability of the nuclei.

In Figure 1.8 a,b), the $(Mw)_{opt}$ versus the temperature, it is possible to observe this characteristic trend [37, 38].

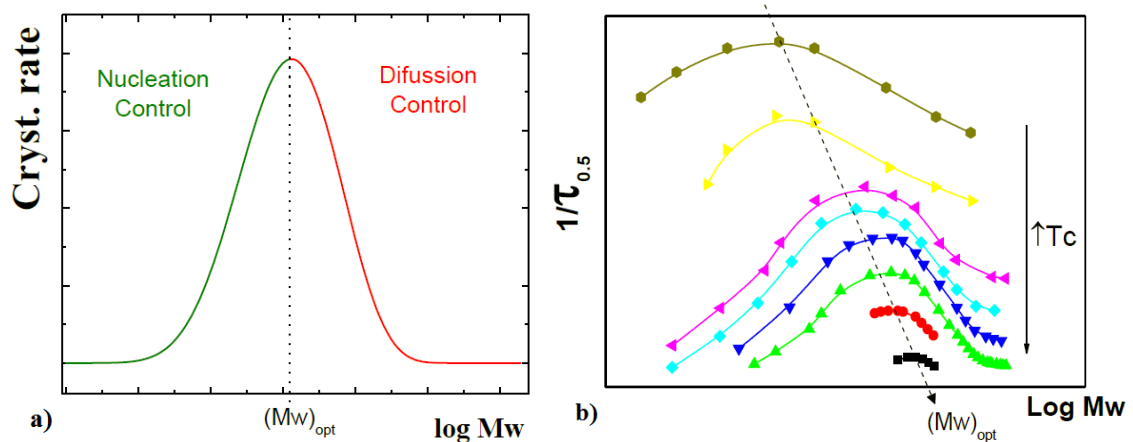


Figure 1.8 a) Overall crystallization rate vs the mass logarithm at $T = \text{const.}$ b) The overall crystallization rate ($1/\tau_{0.5}$) vs. the mass logarithm for different temperatures.^[37]

1.8.1 Avrami theory.

The Avrami theory of crystallization, used initially for compounds with a low molecular weight, is easily applicable to the crystallization of polymers; it allows to obtain information by measuring the development of crystallinity at a constant crystallization temperature.

The Avrami model was used to see how different is the trend of the overall crystallization rate under isothermal conditions of the blends with nanofillers within this thesis.

This theory analyses both the nucleation process and that of crystal growth giving good experimental data during the primary crystallization range, up to approximately 50% conversion.

The following equation represents the Avrami theory of crystallization^[34]:

$$1 - V_c = \exp[-k(t - t_0)^n] \quad \text{Equation 1.1}$$

Where V_c indicates the crystalline volume fraction of the material, k indicates the constant rate of the overall crystallization (contains both the nucleation and the growth), t_0 is the induction time and n is the Avrami index that consists of two parts:

$$n = n_d + n_n \quad \text{Equation 1.2}$$

- Where n_d is the parameter regarding the size of the growing crystal and may show three values 1,2,3 which represent the one - two- three dimension of the crystal. In the case of polymers it is usually common that n_d falls in the values 2, 3 which indicate an axial representation (aggregated lamellae) or spherulites.
- n_n describes the process of nucleation and consists of two values 1,0: 1 when a sporadic nucleation occurs, while 0 is when the nucleation is instantaneous.^[39]

Sporadic nucleation occurs when the rate of spherulite growth is greater than that of nucleation and when the supercooling (i.e. the difference between the melting temperature of the crystals and the temperature of crystallization, $\Delta T = T_m - T_c$) shows low values and there are few but large spherulites.

Instantaneous nucleation, instead, occurs when there are many small spherulites due to the formation at the same instant of many nuclei. This is obtained with a high supercooling where the dominant process is nucleation.

V_c can be calculated with the equation:

$$Vc = \frac{Wc}{Wc + \frac{\rho_c}{\rho_a}(1-Wc)} \quad \text{Equation 1.3}$$

$$Wc = \frac{\Delta H(t)}{\Delta H_{tot}} \quad \text{Equation 1.4}$$

where ρ_a and ρ_c correspond to the density of completely amorphous and completely crystalline polymer respectively; $\Delta H(t)$ corresponds to the enthalpy of crystallization as a function of the crystallization time, while ΔH_{tot} is the overall isothermal crystallization enthalpy of the material.

The equation 1.1 was later re-elaborated by applying logarithmic properties:

$$\log[-\ln(1 - Vc)] = \log(K) + n \log(t - t_0) \quad \text{Equation 1.5}$$

This equation allows to graphically extract both n and K plotting $\log[-\ln(1 - Vc)]$ with the $n \log(t - t_0)$ function. The time required by the material to reach the 50% of crystallization can be indicated as $\tau^{1/2}$ or $\tau_{50\%}$ obtaining the following equation 1.6 [34]:

$$\tau_{1/2} = \left(\frac{-\ln(1-Vc)}{k} \right)^{1/n} = \left(\frac{-\ln(0.5)}{k} \right)^{1/n} \quad \text{Equation 1.6}$$

1.8.2 Lauritzen-Hoffman theory.

The quantitative model of Lauritzen-Hoffman (L-H) allows to predict the crystal growth rate (G). The regime corresponds to the rate of equilibrium of the portion of the chains on the surface. It is divided into:

- Regime I: occurs in the presence of a low supercooling value and when the nucleation rate is very small compared with that of growth
- Regime II: is obtained when the temperature decreases, and therefore there is an increase in the nucleation rate and a decrease in the rate of growth
- Regime III: it has a large supercooling and when the nucleation rate is higher than growth rate.^[38, 40]

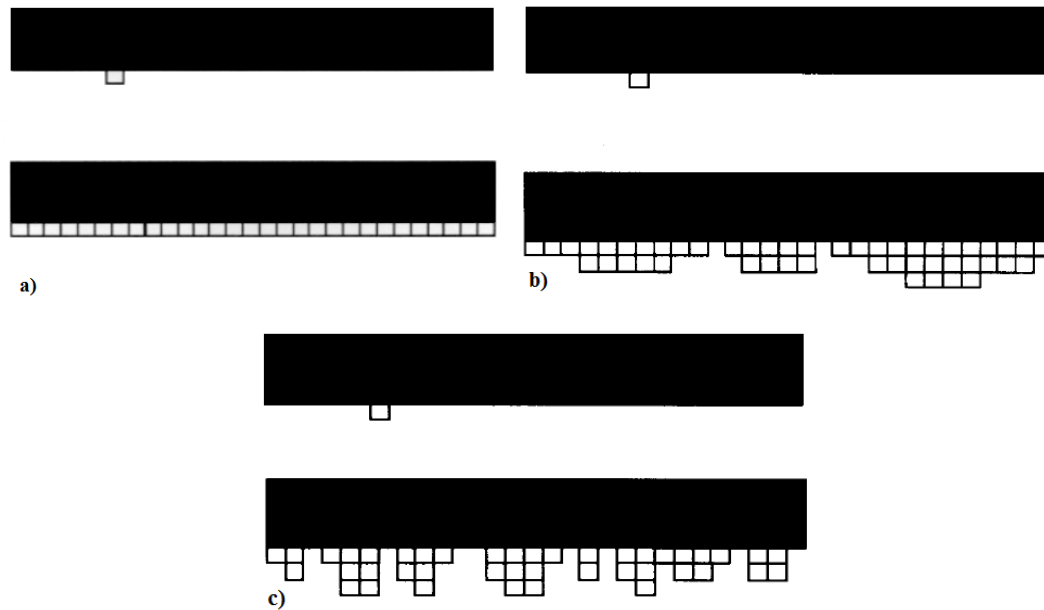


Figure 1.9 Schematic drawings of how polymer crystal growth takes place in three regimes: (a) regime I; (b) regime II; and (c) regime III ^[41].

The following equation describes the rate of crystal growth according to the L-H theory:^[38,40]

$$A(T) = A_0 \exp\left(\frac{-U^*}{R(T_c - T_\infty)}\right) \exp\left(\frac{-K_g^A}{T_c - \Delta T}\right) \quad \text{Equation 1.7}$$

The equation is divided into two parts: the first exponential represents the spread of the chains for the growth process, while the second describes the energy barrier of the secondary nucleation.

A_0 represents a pre-exponential of the rate of growth; U^* the activation energy for the mobility of the chains, R is the universal gas constant, T_c the temperature of isothermal crystallization, $\Delta T = T_m^0 - T_c$ is the supercooling (T_m^0 is the equilibrium melting temperature); T_∞ is the hypothetical temperature where all motion are locked, $T_\infty = (T_g - 30)$ and f is a defined correction factor of the temperature:

$$f = \frac{2T_c}{(T_m^0 + T_c)} \quad \text{Equation 1.8}$$

K_g^A is the nucleation rate constant, which is proportional to the energy barrier for secondary nucleation and is represented by the following mathematical expression:

$$K_g^A = \frac{jb\sigma\sigma_e T_m^0}{k_B \Delta H_m} \quad \text{Equation 1.9}$$

Where j is a constant which depends on the regime of crystallization (it has several values for Regimes I and III, whereas 2 for Regime II); b is the layer thickness, k_B the Boltzmann constant ($1,3806503 \times 10^{-29}$ J/K); ΔH_m is the melting heat; σ_e is the free energy of folding and σ is the lateral surface free energy.

Furthermore, K_g^A can be determined from the Lauritzen-Hofmann graph where $\ln(G) + U^*/R(T_c - T_\infty)$ is reported as a function of $1/(T_c \Delta T)$. (As shown in figure 1.10) [41]

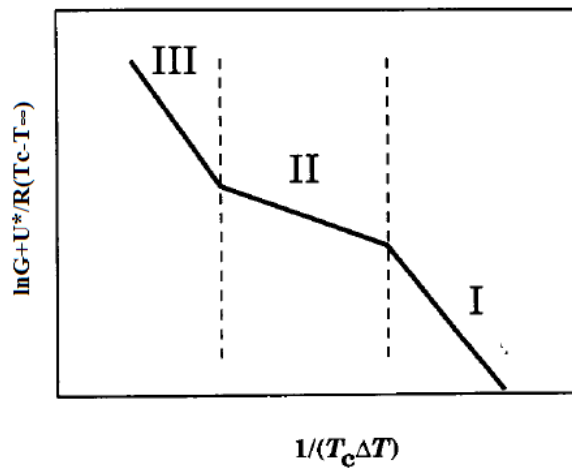


Figure 1.10 Growth rate regimes. [41]

It is possible to calculate also σ_e and q which is the work required for chain bending, using the equations [40] :

$$\sigma = 0.1 \Delta H_m^0 \sqrt{a_0 b_0} \quad \text{Equation 1.10}$$

$$\sigma \sigma_e = \frac{K_g \Delta H_m^0}{j b_0 T_m^0} \quad \text{Equation 1.11}$$

$$q = 2 a_0 b_0 \sigma_e \quad \text{Equation 1.12}$$

Where a_0 is the projection of the chain's longitude, b_0 the width of the chain; each of these parameters depend on the polymer.

2. OBJECTIVE OF THE THESIS

Thermodynamic, physical or mechanical properties of a semi-crystalline polymer, as poly(lactide), PLA, depend on its structure and morphology, therefore, understanding the mechanism of crystallization rate, allows us to understand the behaviour of the polymer.

PLA is a biodegradable thermoplastic polyester and can be produced from renewable sources. However its slow crystallization rate can severely limit its use.

Using of nanocomposite is viewed as an efficient strategy to overcome the aforementioned drawback. Anne-Lise Goffin et al. [9] have highlighted how the cellulose nanowhiskers (CNW) increases PLA crystallization rate. However, the hydrophilic CNW nature does not allow a good compatibility with the hydrophobic polymer matrix of PLA. If the nanocomposites are not homogeneously dispersed, they form micrometric aggregates that don't have effect. One approach to overcome this problem is the exfoliation of the surface of the nanocellulose by grafting the polymer chains. In the present case, "*the grafting from*" is used, because a good degree of exfoliation and high grafting density of nanocellulose are obtained.

This thesis work has investigated the effect of bionanofillers on PLA crystallization rate within in poly(lactide)(PLA)/ poly(caprolactone) (PCL) blend. The used nanofillers are the poly(L-lactide-*co*-caprolactone), poly(L-lactide-*b*-caprolactone) grafted on cellulose nanowhiskers and neat cellulose nanowhiskers. The copolymers were synthesized through the *surface initiated ring opening polymerization* (SI-ROP).

For the synthesis, tin(II) octanoate ($\text{Sn}(\text{Oct})_2$) was used as a catalyst and hydroxyl cellulose nanowhiskers groups as an initiators.

Blends of PLA/nanofillers and PLA/PCL/nanofillers have been prepared by solvent casting. Blends have been characterized by TGA and DSC. TGA analysis allow to evaluate the effect of the nanofillers on the thermal stability of the blends while DSC analysis allow to measure the effect of the nanofillers on the thermal properties of the matrix. The overall crystallization rate of PLA was investigated by both isothermal and non-isothermal DSC.

3. RESULTS AND DISCUSSION

3.1 Synthesis of CNW-g-P(LLA-co-CL) and CNW-g-P(LLA-b-CL) copolymers.

The random poly(L-lactide-co-ε-caprolactone) and block poly(L-lactide-b-ε-caprolactone) grafted on nanocellulose, CNW-g-P(LLA-co-CL) and CNW-g-P(LLA-b-CL), were synthesized through the surface initiated ring opening polymerization (SI-ROP). For the synthesis, it has been used tin(II) octanoate (Sn(Oct)₂) as a catalyst and the hydroxyl cellulose nanowhiskers groups as an initiators. ^[9,43] (As shown in figure 3.1).

In order to optimize the synthesis, a screening of the solvent and the temperature was carried out.

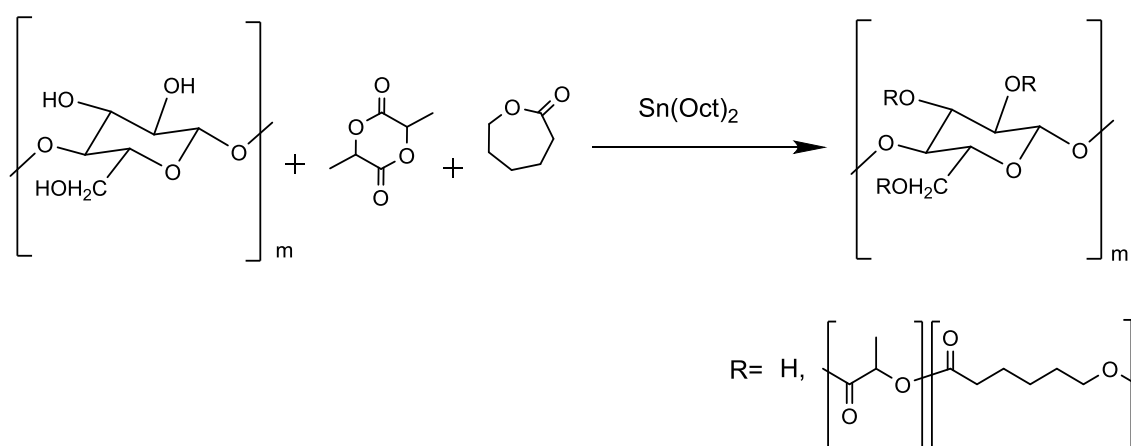


Figure 3.1 Structure of random co-polymer lactide and ε-caprolactone (P(LLA-co-CL)).

Table 3.1 Summary of the synthesis of the copolymers CNW-g-P(LLA-co-CL) and CNW-g-P(LLA-b-CL).

Sample	Time Temp.		LLA/CL	(LLA+CL)/(Sn(oct) ₂)	OH/Sn(oct) ₂	Solvent
	(h)	(°C)				
CNW-g-P(LLA-co-CL) 1	48	120	1	150	2	/
CNW-g-P(LLA-co-CL) 2	16.5	120	1	413	1	/
CNW-g-P(LLA-co-CL) 3	16.5	85	1	413	8	toluene
CNW-g-P(LLA-co-CL) 4	48	85	1	36	0.5	toluene
CNW-g-P(LLA-co-CL) 5	72	85	1	72	1	toluene
CNW-g-P(LLA-co-CL) 6	48	120	1	72	0.9	xylylene
CNW-g-P(LLA-co-CL) 7	48	120	1	403	5.6	xylylene
CNW-g-P(LLA-b-CL) 8	48	85-120	1	106	1.5	xylylene

As shown in the table 3.1, the random copolymer was initially obtained in bulk at 120°C. The reactions carried out in bulk have remarkable advantages: the easiness of the scale up, a lower cost of reaction (there being no solvent) and a lower environmental impact.

The temperature of 120°C was chosen taking into account that at this temperature there is a higher catalytic activity compared to a lower one, with no depolymerization (which may occur at temperatures close to 140°C).

The reaction in bulk, however, has not given the desired results, especially regarding a reduction in the dispersion of nanocellulose: the absence of solvents has not allowed a proper stirring due to the high viscosity of the reaction media (as shown in ATR-IR analysis).

In order to improve the stirring and the dispersion of the copolymer it has been decided to change from the reaction in bulk to that in toluene solution; this implies reduction in temperature from 120°C to 85°C, as shown in the table 3.1, since the boiling point of toluene is 111 °C.

In the reaction in toluene it is noted that the reactivity ratio of the two monomers is not constant during the reaction at 85°C (after in this paragraph will be analyzed in table 3.2). This ratio doesn't allow to obtain a good dispersion in the PLA and/or PCL matrix during the blending process.

In order to obtain a comparable reactivity ratio of the two monomers throughout the reaction time it was decided to increase the reaction temperature from 85°C to 120°C changing the reaction solvent (as shown in the table 3.1).

Indeed it is used xylene as a reaction solvent which has a boiling temperature of 138.5°C and allows to work at 120°C.

After optimizing the synthesis of CNW-g-P(LLA-*co*-CL), the second step was to synthesize a block copolymer taking into account the screening carried out on random copolymers.

It was possible to obtain the block polymer using the different reactivity of the monomers at different temperatures.

Indeed it was decided to synthesize the block poly(L-lactide-*b*-ε-caprolactone) grafted on nanocellulose, CNW-g-P(LLA-*b*-CL), in two different steps: initially, the reaction was conducted at 120°C in xylene for 24 hours with CNW, caprolactone and Sn(Oct)₂, then lactide was added and the temperature lowered to 85°C for 24 hours (as shown in figure 3.2 and in table 3.1).

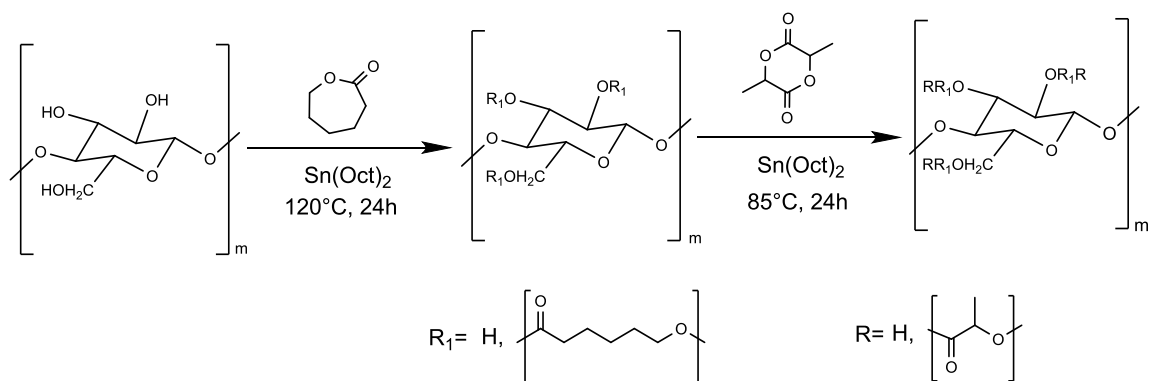


Figure 3.2 Synthesis of block co-polymer lactide and ϵ -caprolactone grafted on cellulose (CNW-g-P(LLA-*b*-CL)).

The lowering of the temperature to 85°C has two positive effects. On one hand it has a high polymerization reactivity of the lactide on the caprolactone, on the other it inhibits the secondary transesterification reaction. Transesterification reaction promotes the formation of random copolymer structure. [44]

Characterization of the random and block copolymers was carried out as follows:

- through nuclear magnetic resonance $^1\text{H-NMR}$ analysis it was possible to determine the final composition of the copolymer, the conversion of the individual polymers and the degree of randomization;
- by attenuated total reflection infrared analysis (ATR-IR) it was possible to determine the actual grafting of the polymer on the nanocellulose;
- with the thermogravimetric analysis (TGA) it was possible to calculate how much the polymer is grafted on the nanocellulose.

3.2 Characterization of CNW-g-P(LLA-*co*-CL) and CNW-g-P(LLA-*b*-CL) copolymers.

The products (CNW-g-P(LLA-*co*-CL) and CNW-g-P(LLA-*b*-CL)) of each reaction were purified by precipitating the reaction mixture into a non-solvent such as ethanol and then hexane (which gave a better separation). Purification is required in order to remove unreacted monomers and the formation of a random copolymer of poly(lactide) and poly(caprolactone) non-grafted on the nanocellulose (P(LLA-*co*-CL) or P(LLA-*b*-CL)).

It was not possible to characterize directly to the $^1\text{H-NMR}$ the product of interest, CNW-g-P(LLA-*co*-CL) or CNW-g-P(LLA-*b*-CL) since it is not soluble in the solvents used for the analysis. Nevertheless, the composition of copolymers depends only on the intrinsic

reactivity of the individual monomer; therefore, with the knowledge of the composition of the non-grafted copolymer, which is perfectly soluble in deuterated chloroform (CDCl_3), it has been possible to quantify the final composition of the grafted copolymer.

The non-grafted copolymer obtained after the evaporation of the solvent and of the non-solvent has been characterized by $^1\text{H-NMR}$, where the presence of characteristic peaks of both monomers has been observed, widened and slightly shifted compared to those corresponding to the monomer; therefore, it is possible to state that both have polymerized. Figure 3.3 shows the spectrum of the non-grafted polymer, P(LLA-*co*-CL).

Characteristic signals for polymerized ϵ -caprolactone (CL) and for polymerized L-lactide (LLA) are:

- the multiplet from 5.05 to 5.25 ppm assigned to methine proton of polymerized L-lactide (2), with some rests of unpolimerized L-lactide at approximately 5.03 ppm;
- the multiplet at 1.56 ppm, to the L-lactide methyl protons (3)
- the multiplet from 4.08 to 4.18 ppm is due to the ϵ -caprolactone (CL) methylene proton that linked to a LLA molecule (9), while the triplet at 4.05 ppm indicates the CL proton linked to another CL molecule (9);
- the multiplet between 2.34 to 2.44 ppm is due to the CL proton that linked to a LLA molecule (5), while the triplet at 2.30 indicates that the CL proton linked to another CL molecule (5);
- for the rest of the spectrum, multiplets at 1.66 ppm and 1.39 ppm are related to the CL protons (6, 7, and 8), respectively^[45](as shown in figure 3.3).

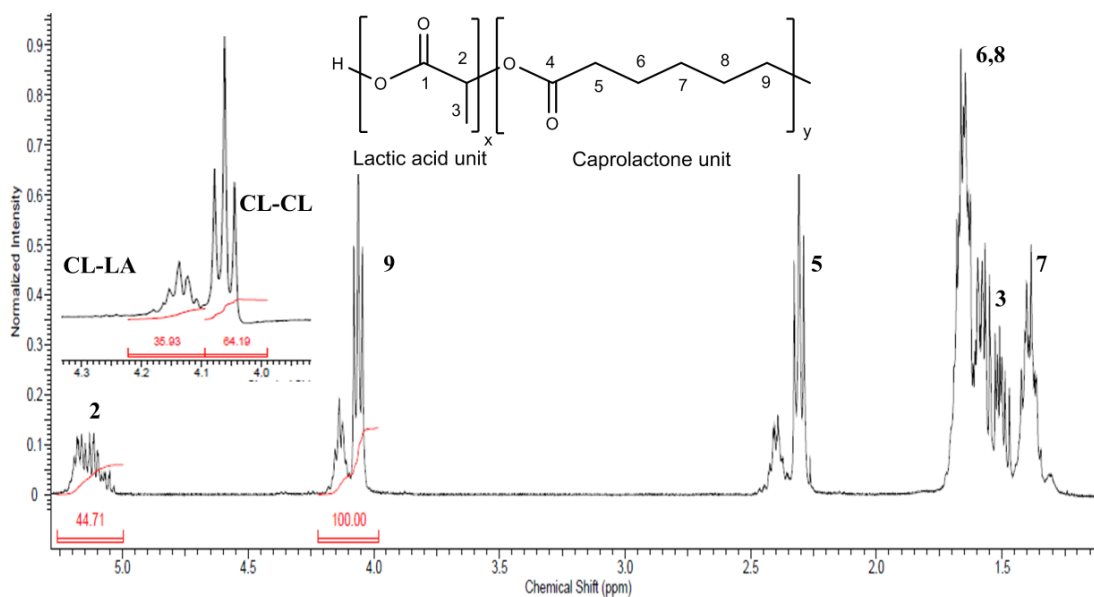


Figure 3.3 $^1\text{H-NMR}$ (400MHz) spectrum of the P(LLA-*co*-CL) in CDCl_3 .

Figure 3.4 shows the spectrum of the non-grafted fraction of the CNW-g-P(LLA-*b*-CL) which confirms the formation of the block copolymer; in fact there are no two triplets from 4.05 ppm to 4.18 ppm, typical of a random copolymer, but there is only one triplet at 4.05 ppm which indicates that the CL proton is linked to another CL molecule (9), like in a block copolymer.

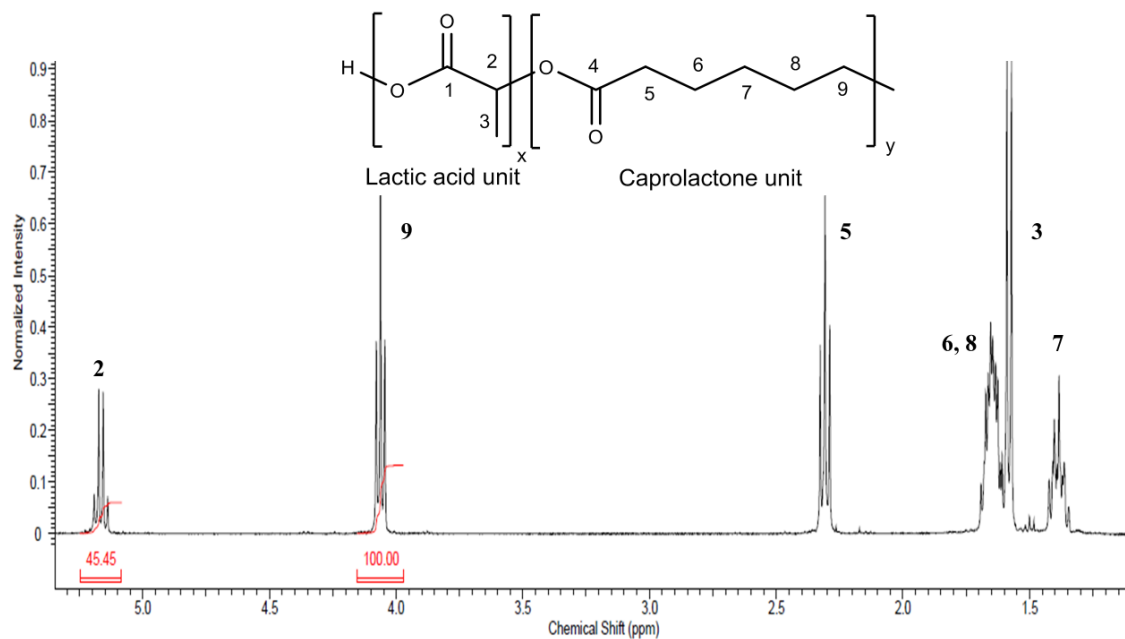


Figure 3.4 ¹H-NMR (400MHz) spectrum of the P(LLA-*b*-CL) in CDCl₃.

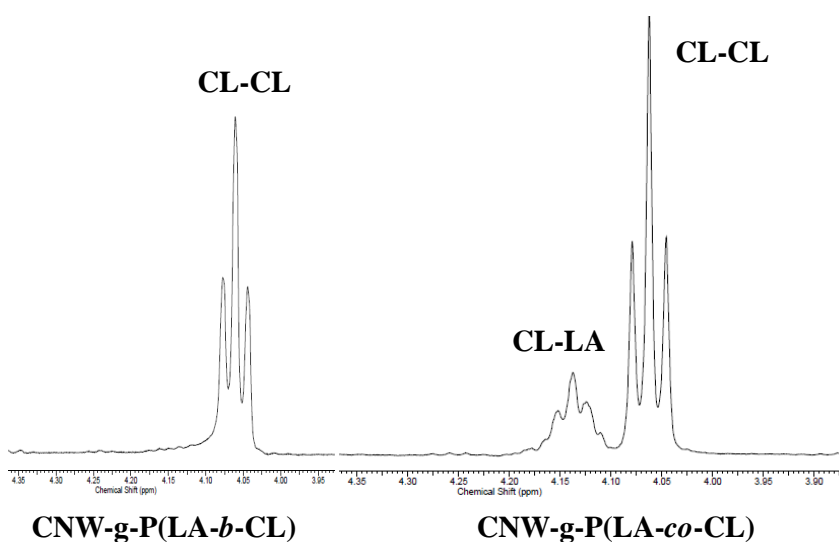


Figure 3.5 ¹H-NMR (400MHz) spectrum zoom of P(LLA-*b*-CL) and P(LLA-*co*-CL) in xylene in CDCl₃

Thanks to the $^1\text{H-NMR}$ analysis it was possible to determine the final composition of the copolymer, the conversion of the individual polymers and the randomization degree. (As shown in Table 3.2).

The final composition of the copolymer was calculated from the ratio of the methyne lactide proton integral (5.15 ppm) and the sum of the integral of the latter with integral of the methylene proton of the caprolactone (4.10 ppm).

The conversion in the poly(lactide) and in the poly(caprolactone) was calculated as the ratio of the integral of the proton of the polymer and the sum of the latter with integral of the same proton of unreacted monomer (which falls to the lowest chemical shift in the case of lactide and higher in the case of caprolactone).

Finally, the degree of randomization with the ratio of the integral of the multiplet of caprolactone (4.18 to 4.08 ppm) is determined.

3.2 Table conversion and composition of CNW-g-P(LLA-*co*-CL) and CNW-g-P(LLA-*b*-CL)

Sample	Conversion CL (%)	Conversion LLA (%)	Composition		Random.
			CL (%)	LLA (%)	degree (%)
CNW-g-P(LLA- <i>co</i> -CL) 1	87	89	55	45	29
CNW-g-P(LLA- <i>co</i> -CL) 2	23	81	54	46	32
CNW-g-P(LLA- <i>co</i> -CL) 3	49	96	38	62	28
CNW-g-P(LLA- <i>co</i> -CL) 4	93	100	51	49	25
CNW-g-P(LLA- <i>co</i> -CL) 5	94	100	61	39	27
CNW-g-P(LLA- <i>co</i> -CL) 6	100	100	53	47	16
CNW-g-P(LLA- <i>co</i> -CL) 7	99	97	54	46	28
CNW-g-P(LLA- <i>b</i> -CL) 8	100	98	55	45	0

In the table 3.2 the conversion of the copolymers indicates high values for all the copolymers, except P(LLA-*co*-CL) 2 and P(LLA-*co*-CL) 3, which have not enough time to react.

Regarding the composition we can see that for products in bulk there is a composition of approximately 55 % of caprolactone and 45 % of lactide; for copolymer in toluene there are different composition depending on reaction time (as shown in table 3.2).

Indeed figure 3.6 and in table 3.2 below show the different reactivity of the copolymer of P(LLA-*co*-CL) 3. In these conditions, the composition of copolymer is different to feed composition. In particular, the percentage for lactide is about 62% while for caprolactone is 38%.

At this temperature, the reactivity ratio of the two monomers is not same.

In order to obtain a comparable reactivity ratio of the two monomers throughout the reaction time it was decided to increase the reaction temperature from 85°C to 120°C, changing the reaction solvent, xylene.

The synthesis in xylene at 120°C turn out to be better one, thanks to the correct composition (50/50) of the grafted. The 50/50 composition allows to obtain a better dispersion of the bionanofillers in the PLA and/or PCL matrix.

The degree of randomization is approximately 30%, except for the CNW-g-P(LLA-*co*-CL) 6, 16%, and for the CNW-g-P(LLA-*b*-CL), which, since being block copolymer, the degree of its randomization is 0%.

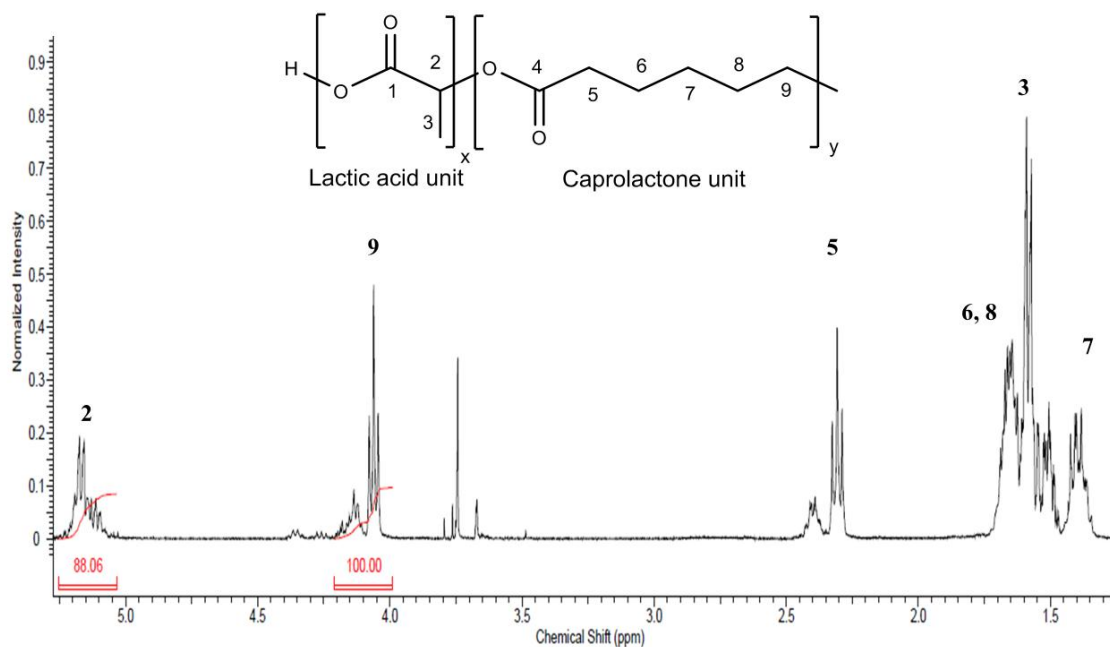


Figure 3.6 $^1\text{H-NMR}$ (400MHz) spectrum of P(LLA-*co*-CL) 3 in toluene in CDCl_3

In order to determine the physical-chemical properties and structural properties of a solid material infrared spectroscopy analysis is generally used; in the case of our product it is not possible to apply this type of analysis since it is an opaque powder. To overcome this problem it is possible to use the attenuated total reflectance, better known as ATR-IR.

The ATR-IR analysis allowed to determine the effective grafting of the polyesters on nanocellulose. The nanocellulose characteristic bands of ATR-IR spectrum are:

- from 3650 cm^{-1} to 3200 cm^{-1} which is due to the hydroxyl O-H groups stretching vibration of cellulose;

- at 2902 cm^{-1} that corresponds to the stretching of asymmetric and symmetric methyl and methylene C–H groups;
- at 1337 cm^{-1} that could be assigned as the C–OH bending;
- at 1160 cm^{-1} that is attributed to C–O–C bending;
- at 897 cm^{-1} which is due to the C–O–C asymmetric stretching at the β -(1 \rightarrow 4)-glycosidic linkage.

The CNW-g-P(LLA-*co*-CL) and CNW-g-P(LLA-*b*-CL) characteristic bands of ATR-IR spectrum are:

- at 3017 cm^{-1} that could be assigned as methyl group stretching of lactide;
- from 3200 cm^{-1} to 2850 cm^{-1} that correspond to methylene group stretching of caprolactone and to the broad characteristic band of cellulose.
- at 1750 cm^{-1} that corresponds to carbonyl C=O stretching vibration of lactide;
- at 1728 cm^{-1} which is assigned to the carbonyl C=O stretching vibration of caprolactone. ^[43]

The validation of the copolymer grafting is given by the presence of one or two bands (depending on whether it is a random or block copolymer) from 1750 cm^{-1} to 1728 cm^{-1} . The figure 3.7 shows the analysis of different samples.

The copolymer CNW-g-P(LLA-*co*-CL) is characterized by a single broad band at about 1733 cm^{-1} , while the copolymer CNW-g-P(LLA-*b*-CL) shows two partially overlapping bands that have two maxima, 1748 cm^{-1} attributable to the stretching of the carbonyl group of the L-lactide, and the other at 1728 cm^{-1} to that of the caprolactone. (As shown in figure 3.7 c))

The rise of the band intensity from 1750 cm^{-1} to 1728 cm^{-1} shows a higher grafting thus improving compatibility between the cellulose hydrophilic and the hydrophobic polymer matrix.

In bulk copolymer there characteristic bands of copolymer grafted are practically reduced to zero. This fact can be caused by reduction in the dispersion of nanocellulose in the reaction media given high viscosity and grafting can not be efficiently. In order to improve the stirring and the dispersion of the copolymer, it has been decided to change from the reaction in bulk to that in toluene solution at 85°C.

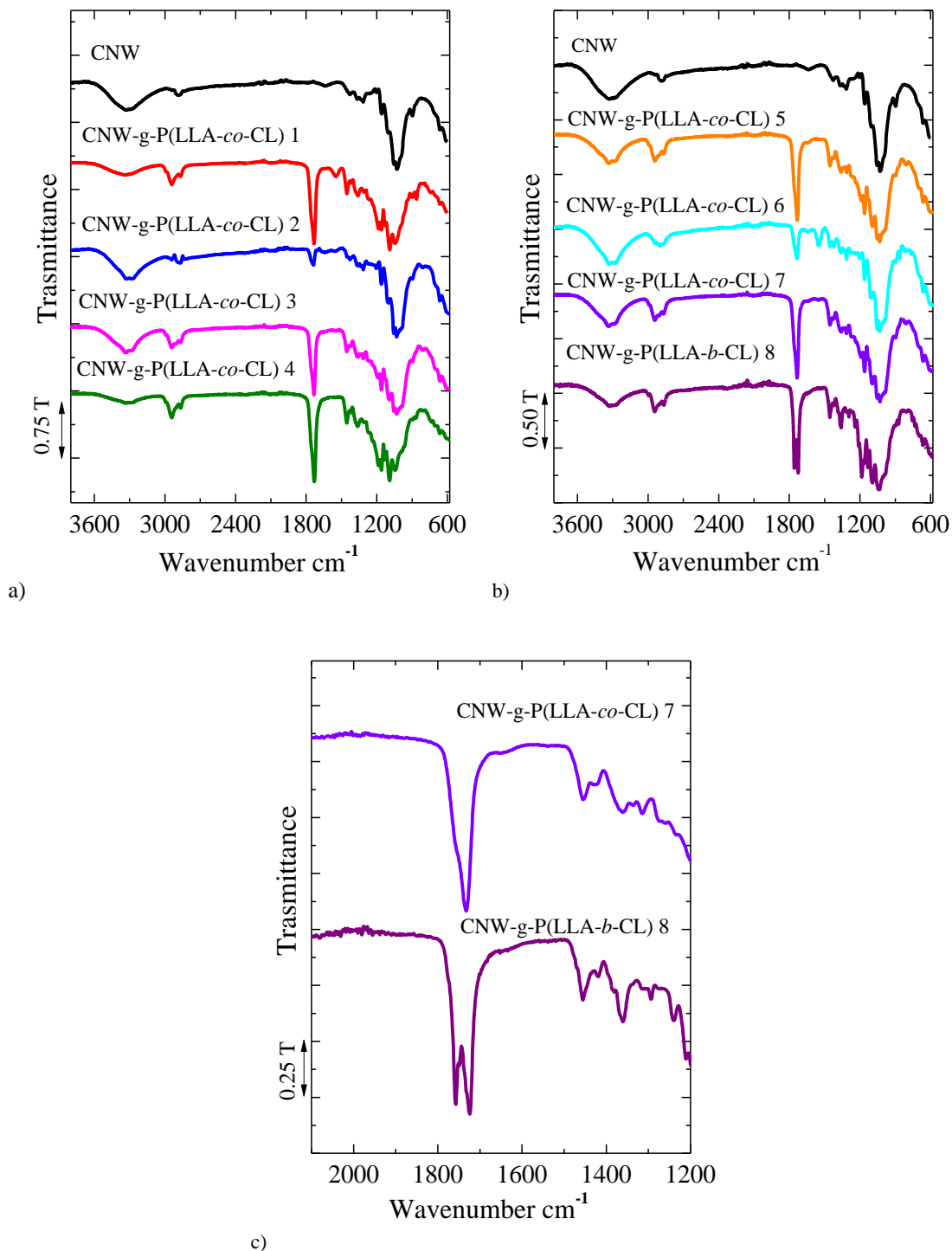


Figure 3.7 a) ATR-IR spectrum of the CNW-g-P(LLA-*co*-CL) 1, 2, 3, 4 and CNW, b) ATR-IR spectrum of the CNW-g-P(LLA-*co*-CL)5,6,7, CNW-g-P(LLA-*b*-CL) 8 and CNW c) ATR-IR spectrum zoom of the CNW-g-P(LLA-*co*-CL) and CNW-g-P(LLA-*b*-CL) in xylene.

Finally, we studied thermal degradation behaviour of copolymers CNW-g-P(LLA-*co*-CL) and CNW-g-P(LLA-*b*-CL) by thermogravimetric analysis (TGA). This measure aims mainly at determining the copolymer composition and defining the thermal stability of the

materials. This technique is able to characterize materials which show mass losses due to thermal decomposition, oxidation (working in an oxidizing atmosphere) or physical processes such as evaporation and stripping.

The measurements in this work were conducted in a nitrogen atmosphere from 40 °C to 600 °C using a heating rate modulated by the derivative before the loss of mass; the faster is the decomposition of the sample the lower is the heating rate. This method allows to have a better resolution since the copolymer and the nanocellulose have similar thermal degradation trends.

The graphs show the weight losses of CNW, CNW-g-P(LLA-*co*-CL) and CNW-g-P(LLA-*b*-CL) as function of temperature. (As shown in figures 3.8 and 3.9)

Thermal degradation of nanocellulose proceeds in two steps between 280°C and 330°C (with a maximum degradation placed at 296°C) as a result of depolymerization, dehydration and decomposition of glycosyl units present in cellulose, yielding a char residue of 25 wt.%.^[43]

When lactide and caprolactone chains are grafted on nanocellulose there are two different stages of thermal degradation, starting from 278°C to 300°C and obtain maximum degradation rate at about among 300°C and 310°C.^[44]

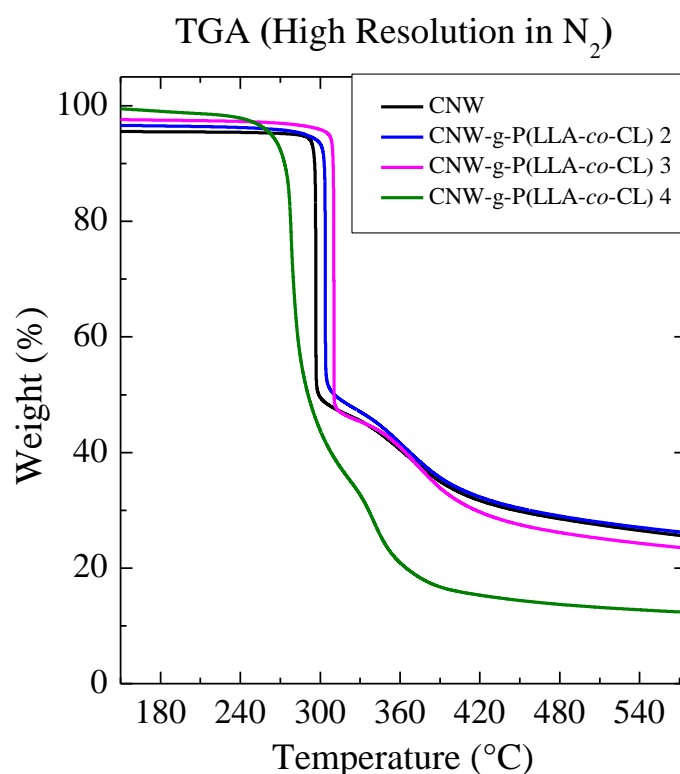


Figure 3.8 Thermogravimetric analysis of CNW, CNW-g-P(LLA-*co*-CL) 1, 2, 3, 4 in N₂ atmosphere.

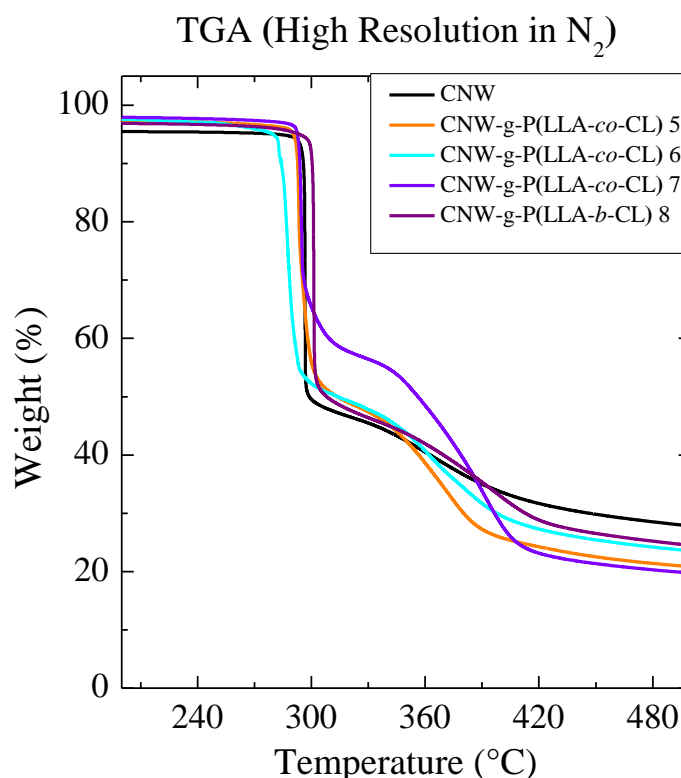


Figure 3.9 Thermogravimetric analysis of CNW, CNW-g-P(LLA-co-CL) 5, 6, 7 and CNW-g-P(LLA-b-CL) 8 in N₂ atmosphere.

Table 3.3 show the percentage of weight of the copolymer (w%) and the temperatures of the thermal degradation: the temperature at which degradation starts (T_{onset}), the temperature at 10% of weight loss (of T lost 10% w.) and the temperature at which the maximum degradation (T_{max} (°C) degradation rate) occurs; the first two were determined graphically while the last by the first derivative of the curve weight loss/time.

Thermogravimetric analysis allowed to calculate the percentage of polymer grafted on nanocellulose with the following equation:

$$\% \text{ polymer grafted} = \frac{\text{CNW residue (\%)} - \text{copolymer residue (\%)}}{\text{CNW residue (\%)}} * 100 \quad \text{Equation 3.1}$$

The non-grafted copolymer (P(LLA-co-PCL) and P(LLA-b-CL)) has a residue of 0%, while the nanocellulose has a residue of 25%, the residue of the grafted copolymer corresponds to the cellulose within it.

In the table 3.3 the copolymers CNW-g-P(LLA-co-CL) 2 and 3 show a percentage of grafted polymer lower than 10% since the polymerization has not had sufficient time to react; the other copolymers show a percentage between 20% and 30%, except the CNW-

g-P(LLA-*co*-CL) 4, 50%, given the high level of catalyst and of the CNW-g-P(LLA-*b*-CL) 8, 10%.

Table 3.3 TGA analysis of CNW-g-P(LLA-*b*-CL), CNW-g-P(LLA-*co*-CL).

Sample	Tonset (°C)	T of lost 10 w%. (°C)	T max degradation rate (°C)	w%. Polymers
CNW	280	296	296	/
CNW-g-P(LLA- <i>co</i> -CL) 2	278	303	304	1
CNW-g-P(LLA- <i>co</i> -CL) 3	297	310	310	6
CNW-g-P(LLA- <i>co</i> -CL) 4	225	273	279	50
CNW-g-P(LLA- <i>co</i> -CL) 5	285	293	296	23
CNW-g-P(LLA- <i>co</i> -CL) 6	245	287	288	20
CNW-g-P(LLA- <i>co</i> -CL) 7	270	294	293	30
CNW-g-P(LLA- <i>b</i> -CL) 8	263	300	301	10

Figure 3.10 shows that as the amount of the catalyst increases we have a greater thermal instability; it is hypothesized that this is caused by an increase in the rate of degradation induced by the residual tin present in the catalyst (which is not possible to completely eliminate).^[44]

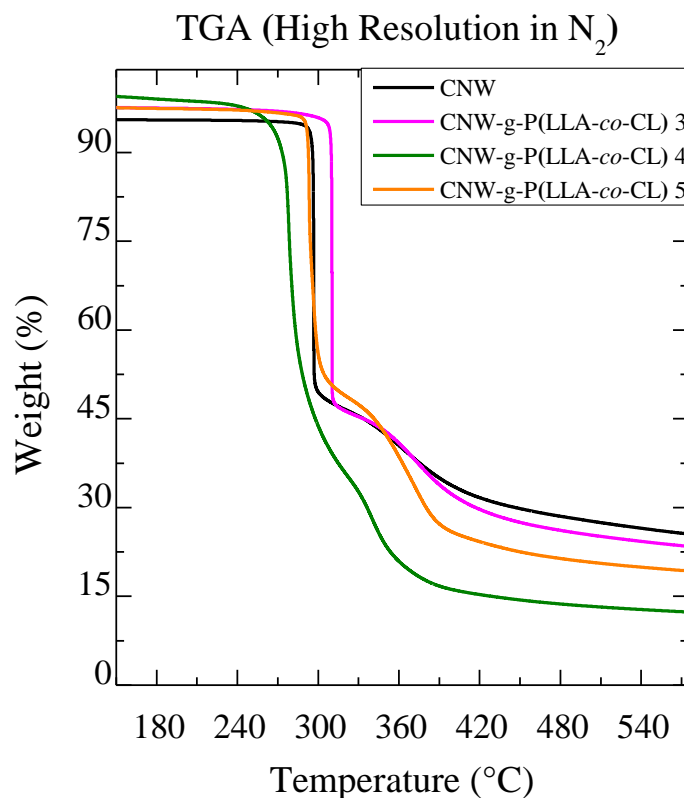


Figure 3.10 Thermogravimetric analysis of CNW-g-P(LLA-co-CL) 3,4,5 and CNW in N₂ atmosphere.

3.3 Preparation of the blends.

The second part of the thesis is divided in two sections:

- preparation of the poly(lactide)(PLA)/poly(caprolactone)(PCL)/nanofillers 100/0/5 and 80/20/5 blends and their physical and chemical characterization;
- study of the overall crystallization rate of the PLA phase in neat PLA and in the 80/20 PLA/PCL blend in the presence of the synthesized copolymers and nanocellulose, in order to verify if the presence of the copolymer effects on the rate of crystallization; Avrami's equation and the theory of Lauritzen-Hoffman were used.

The copolymers selected after screening in paragraph 3.1 were CNW-g-P(LLA-co-CL) 7 and CNW-g-P(LLA-b-CL) 8.

The preparation of the blends were carried out through the solubilisation of homopolymers of PLA and PCL, in a solution of dichloromethane (total concentration 1g/dL).

Six blends were prepared: three are neat PLA and other are PLA/PCL 80/20, after CNW-g-P(LLA-co-CL) or CNW-g-P(LLA-b-CL) or nanocellulose were respectively added in the blends, as shown in table 3.4.

Blends were homogenized in an ultrasound for 10 minutes. Ultrasound was indispensable for a greater dispersion of the copolymer in the PLA and PLA/PCL matrix making the blend homogeneous.

Compositions studied here are 100/0/5, 80/20/5 PLA, PCL and nanofillers (CNW, CNW-g-P(LLA-co-CL) and CNW-g-P(LLA-b-CL)). (As shown in Table 3.4).

Table 3.4 Composition of blends

Polyester		Composition in weight	
matrix	nanofillers	PLA/PCL/nanofiller	% CNW weight
PLA/PCL	CNW	100/0/5	5%
PLA/PCL	CNW	80/20/5	5%
PLA/PCL	CNW-g-P(LLA-co-CL)	100/0/5	3.5%
PLA/PCL	CNW-g-P(LLA-co-CL)	80/20/5	3.5%
PLA/PCL	CNW-g-P(LLA-b-CL)	100/0/5	4.5%
PLA/PCL	CNW-g-P(LLA-b-CL)	80/20/5	4.5%

3.4 Thermogravimetric analysis of blends.

Thermograms show in figure 3.11 were obtained by thermogravimetric analysis (TGA), under nitrogen from 40°C to 600°C using heating rate high resolution technique. This technique used a heating rate modulated by the derivative before the loss of mass, which allows to have a better resolution.

Figure 3.11 shows the thermal behaviour of following blends:

- PLA;
- PLA/CNW 100/5;
- PLA/CNW-g-P(LLA-co-CL) 100/5;
- PLA/CNW-g-P(LLA-b-CL) 100/5.

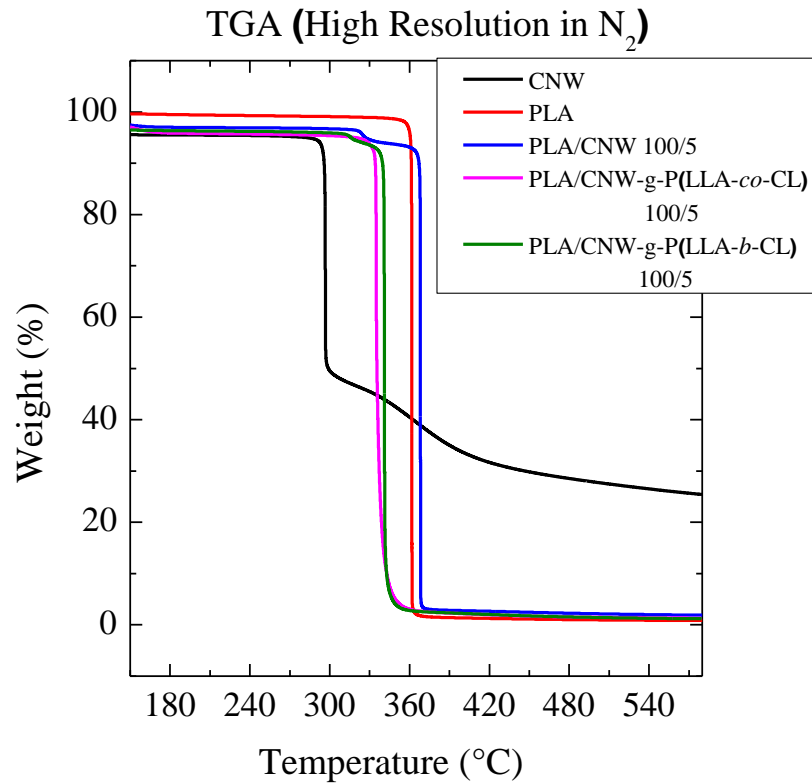


Figure 3.11 Thermogravimetric analysis of CNW, PLA, PLA/CNW 100/5, PLA/CNW-g-P(LLA-co-CL) 100/5 and PLA/CNW-g-P(LLA-b-CL) 100/5 in N₂ atmosphere.

TGA analysis allows to determine quantitatively the blends composition, further it gives us more information about the relative thermal stability and the overall behaviour of the degradation process. In the thermal analysis of PLA blends various aspects are noticeable. Table 3.5 shows that a thermal shift between 330°C and 368°C, which is attributable to the degradation temperature of PLA, occurs depending on the blend.

Thermogram of PLA/CNW 100/5 (as shown in table 3.5) has a 320°C lapse which may indicate the degradation of nanocellulose within the blend.

Table 3.5 TGA analysis of neat PLA, PLA/CNW 100/5, PLA/CNW-g-P(LLA-*co*-CL) 100/5 and PLA/CNW-g-P(LLA-*b*-CL) 100/5.

Sample	Tonset (°C)	T of lost 10 w% (°C)	T max degrad.rate (°C)
PLA	348	361	360
PLA/CNW 100/5	316	367	368
PLA/CNW-g-P(LLA- <i>co</i> -CL) 100/5	294	330	334
PLA/CNW-g-P(LLA- <i>b</i> -CL) 100/5	286	340	339

In the blend containing CNW-g-P(LLA-*co*-CL) and CNW-g-P(LLA-*b*-CL) a faster rapid degradation than other blends occurs, i.e. the thermal stability decreases. (As shown in table 3.5)

This behaviour may be caused by the lower packing rate of the grafted copolymers compared with nanocellulose. It is hypothesized that the grafted copolymer chains interpose between the layers of nanocellulose modifying the structure and thereby increasing sensitivity to thermal degradation. [43,45]

In addition, in blends with grafted copolymers, the copolymer increases the interaction between nanocellulose and polymer matrix. Indeed, there isn't a step of nanocellulose at 320°C.

The figure 3.12 shows the thermal degradation of following blends:

- PLA/PCL 80/20;
- PLA/PCL/CNW 80/20/5;
- PLA/PCL/CNW-g-P(LLA-*co*-CL) 80/20/5;
- PLA/PCL/CNW-g-P(LLA-*b*-CL) 80/20/5.

The performance of the thermograms, as shown in figure 3.12 and in table 3.6.

It is possible to assume, two thermal steps, since the polymers in blends are immiscible so their intrinsic degradability act independently between each other. Since PCL has a greater thermal stability than PLA, it is possible to attribute the thermal degradation of poly(lactide) (which occurs between 334°C and 340°C) to the first step, and to the weight loss of the poly(caprolactone) (which occurs at about 358°C) to the second. [44]

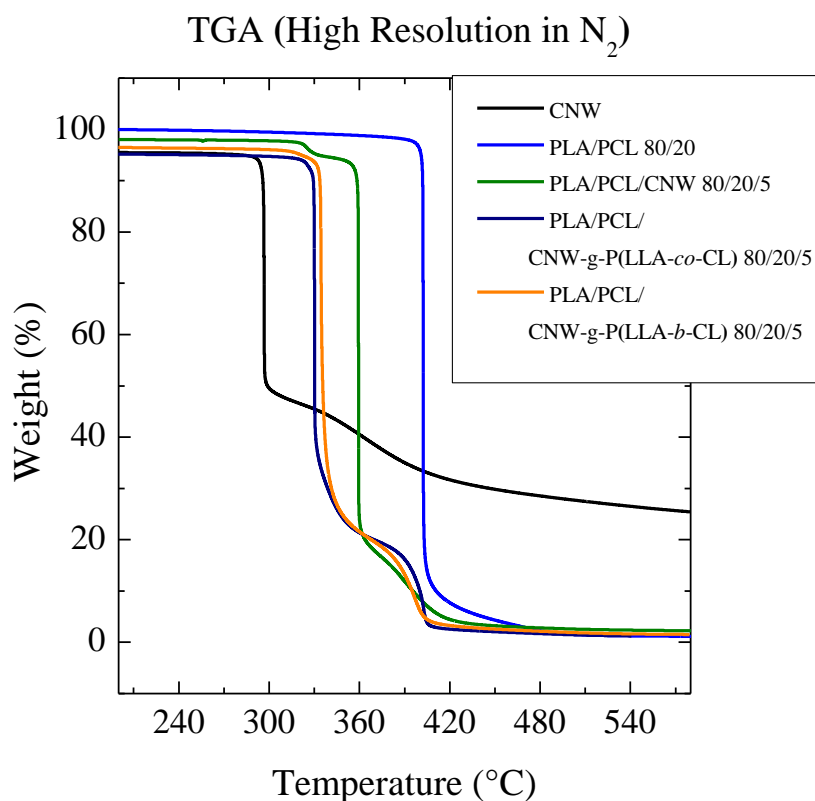


Figure 3.12 Thermogravimetric analysis of CNW, PLA/PCL 80/20, PLA/PCL/CNW 80/20/5, PLA/PCL/CNW-g-P(LLA-*co*-CL) 80/20/5 and PLA/PCL/CNW-g-P(LLA-*b*-CL) 80/20/5 in N₂ atmosphere.

As in the previous case also for the PLA/PCL/CNW 80/20/5 blend there is a peak at 320°C attributable to the degradation of nanocellulose. The blends with random and block copolymers have a lowering of thermal stability. Experimental data, as shown in the table 3.6, confirms the composition by weight of blend polymers.

Table 3.6 TGA analysis of CNW, PLA/PCL 80/20, PLA/PCL/CNW 80/20/5, PLA/PCL/CNW-g-P(LLA-*co*-CL) 80/20/5 and PLA/PCL/CNW-g-P(LLA-*b*-CL) 80/20/5.

Sample	Tonset (°C)	T of lost 10 w% (°C)	T max degrad.rate (°C)	PLA w%	PCL w%
PLA/PCL 80/20	355	358	357	80	20
PLA/PCL/CNW 80/20/5	314	358	359	80	20
PLA/PCL/CNW-g-P(LLA- <i>co</i> -CL) 80/20/5	308	329	330	80	20
PLA/PCL/CNW-g-P(LLA- <i>b</i> -CL) 80/20/5	290	334	336	80	20

3.5 Differential scanning calorimetry (DSC): non-isothermal crystallization.

The thermal properties of the polymers were determined using DSC. Scans taken from the first heating, the cooling and the second heating are reported for nanofillers (CNW, CNW-g-P(LA-*co*-CL) and CNW-g-P(LA-*b*-CL)), neat PLA, neat PCL, and all blends.

The first heating scan is used to eliminate the thermal history of the sample. All tests were performed at 10°C/min in a temperature range between -20°C and 200°C. Figure 3.13 shows the CNW, CNW-g-P(LLA-*co*-CL) and CNW-g-P(LLA-*b*-CL) which have a different behaviour.

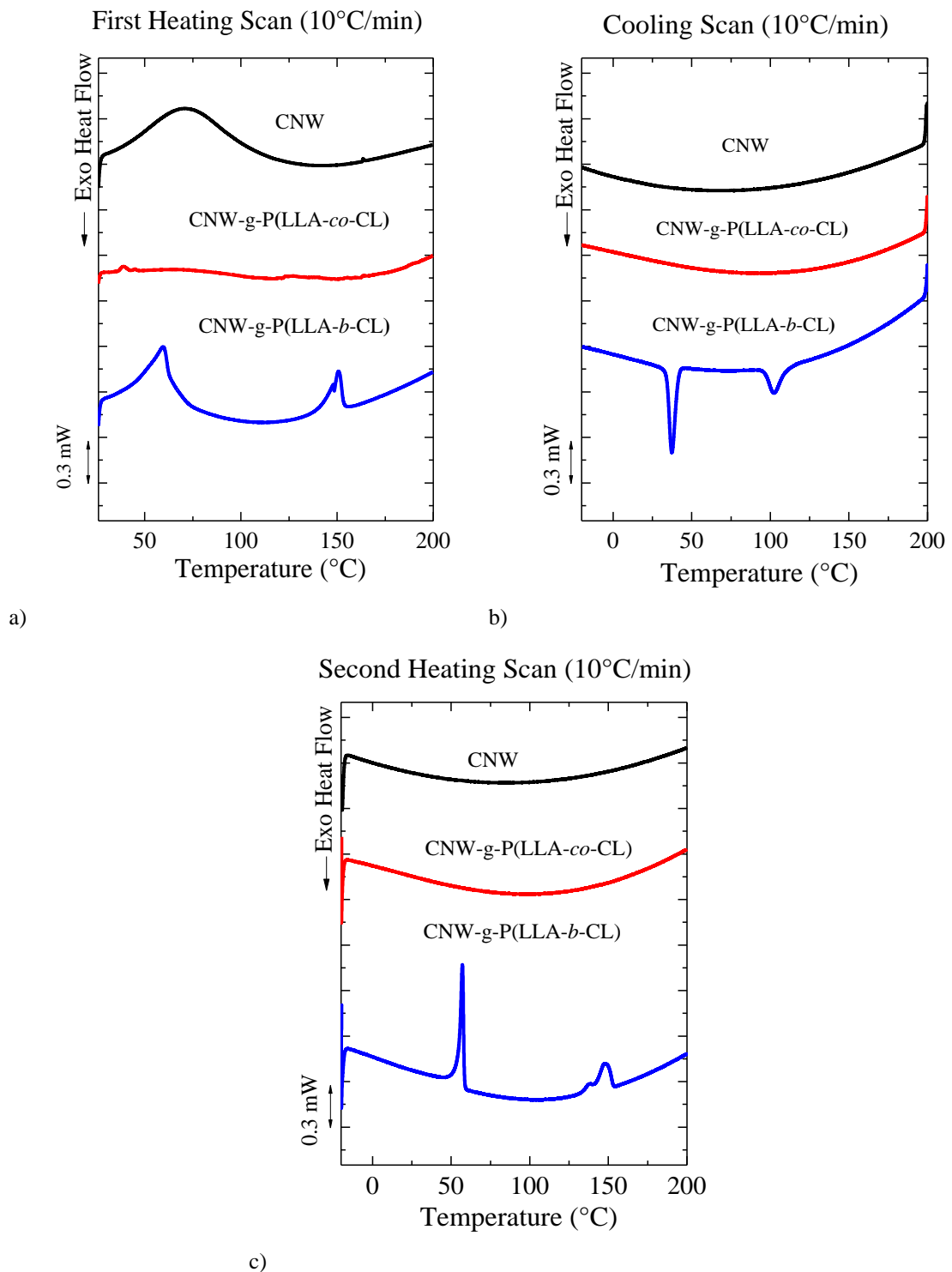


Figure 3.13 DSC first heating scan. *b)* DSC Cooling scan from the melt following the first heating scan shown in a) *c)* Subsequent DSC second heating scan after the cooling run shown in b) for CNW, CNW-g-P(LLA-co-CL) and CNW-g-P(LLA-b-CL).

The table 3.7 shows data of cooling and the second heating scans: the peak of cold crystallization temperature (T_{cc}), the enthalpy of crystallization (ΔH_c), the enthalpy of

cold crystallization (ΔH_{cc}), the peak melting temperature (T_m) and the enthalpy of fusion (ΔH_m).

In the CNW-g-P(LLA-*b*-CL) cooling scans there are two exothermic peaks, one at 37°C which corresponds to the temperature of crystallization of the PCL and the other one at 102°C regarding the PLLA.

The PLLA within copolymer show a crystallization during the cooling scan because it is present in long sequences in the L-form. Instead, commercial PLA shows its slow crystallization rate, due to the low presence of D-isomer in the material.

CNW-g-P(LA-*co*-CL) shows no exothermic peak.

In second heating scans, there are two endothermic peaks of the melting temperatures in the block copolymer; the first corresponds to PCL at 56°C and the second to PLA at 148°C.

Table 3.7 DSC data obtained from figure 3.13 CNW, CNW-g-P(LLA-*co*-CL) and CNW-g-P(LLA-*b*-CL).

Sample	Cooling scan				Second heating scan			
	PCL cryst.		PLA cryst.		PCL melting		PLA melting	
	T_{cc} (°C)	ΔH_{cc} (J/g)	T_{cc} (°C)	ΔH_{cc} (J/g)	T_m (°C)	ΔH_m (J/g)	T_m (°C)	ΔH_m (J/g)
CNW	-	-	-	-	-	-	-	-
CNW-g-P(LLA- <i>co</i> -CL)	-	-	-	-	-	-	-	-
CNW-g-P(LLA- <i>b</i> -CL)	37	16.5	102	9.7	56	17.3	148	9.6

The crystallization of a block copolymer occurs from a single phase either in the melt or in a weakly segregated melt.^[46]

In random copolymers with this composition (50% mol of LA and 50% mol of CL), instead, a crystalline phase cannot be achieved, because there is a random distribution of the repeating units. All the thermal transitions (T_c and T_m) of PLA within CNW-g-P(LLA-*b*-CL), are obtained at lower temperature than neat PLA. This is caused by low molecular weight of grafted chains in comparison with neat PLA.

The figure 3.14 shows the scans of following samples:

- neat PLA;
- PLA/CNW 100/5 blend;
- PLA/CNW-g-P(LLA-*co*-CL) 100/5 blend;
- PLA/CNW-g-P(LLA-*b*-CL) 100/5 blend.

The figure 3.14 b) and the table 3.8 of the second heating scans show three important features. Firstly, their respective PLA glass transition temperatures (T_g) of the blends fall

in range between 60°C and 63°C. Secondly, the exothermic peaks between 100°C and 120°C are attributed to cold crystallizations of the PLA. Thirdly, the endothermic peaks, between 162°C and 169°C, are caused by the melting temperature of the PLA in the blends.

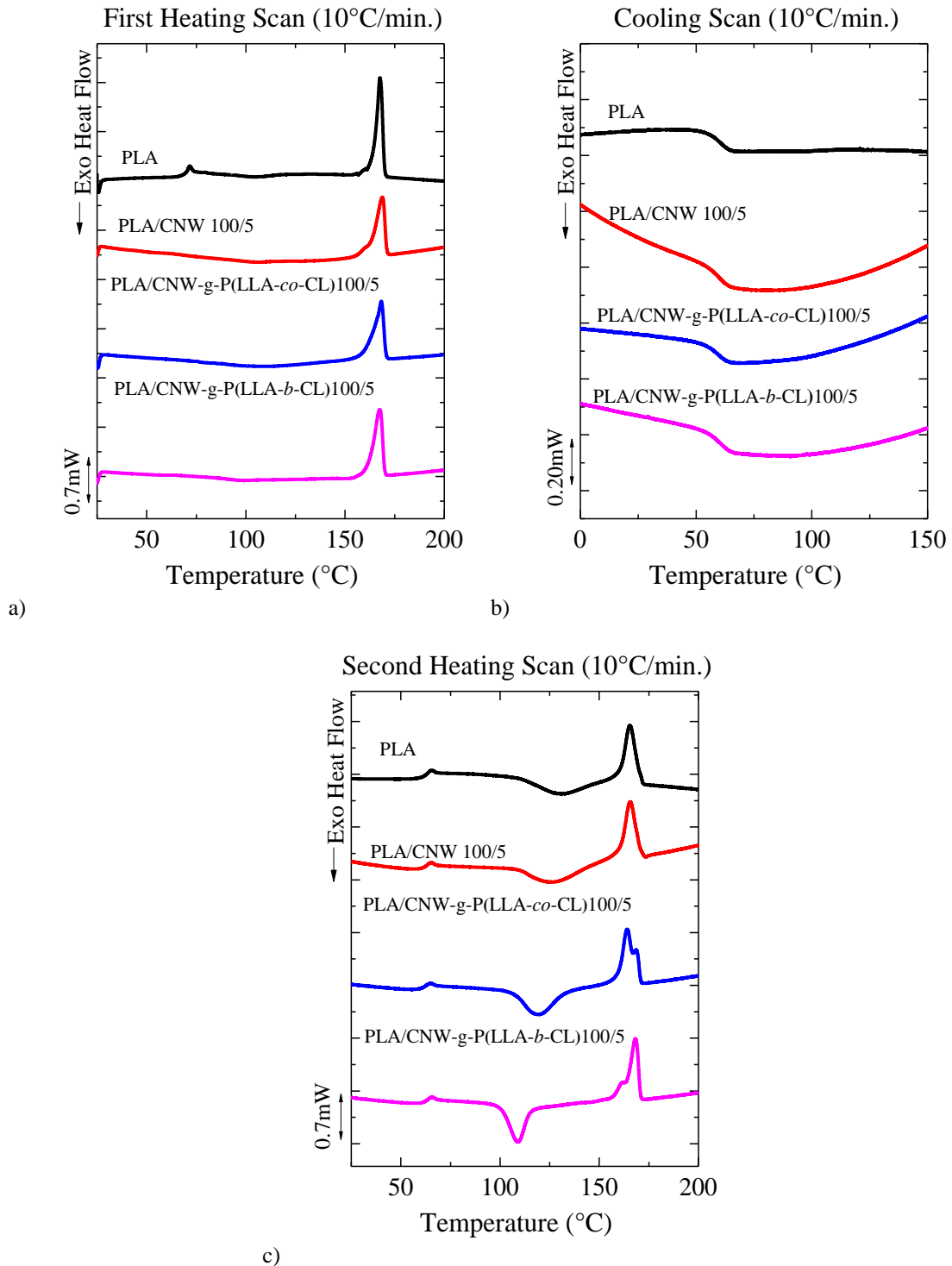


Figure 3.14 DSC first heating scan. *b)* DSC Cooling scan from the melt following the first heating scan shown in a) *c)* Subsequent DSC second heating scan after the cooling run shown in b) for PLA, PLA/CNW 100/5, PLA/CNW-g-P(LLA-co-CL) 100/5 and PLA/CNW-g-P(LLA-b-CL) 100/5.

The glass transition temperatures of PLAs haven't remarkable changes. The Tg may have two opposite effects: on one hand the grafted PLLA chains has plasticization effect on the matrix, on the other hand nanocellulose acts as non-plasticizer. Both behaviours have limited effect due to low percentage of copolymer within matrix.

Regarding the exothermic peak, the cold crystallization occurs as expected at much higher temperatures than the Tg of PLA (close to 60°C).

It is hypothesized that the absence of previous PLA crystallization is due to a slow crystallization rate during previous cooling, furthermore, cooling PLA through its glass transition temperature (Tg), generally causes the formation of nuclei that can later be employed during heating for cold crystallization purposes. Crystals formed by cold crystallization during the scan also exhibit clear melting peaks (figure 3.14 c)).

Moreover, lowering of crystallization temperature indicates that random and block copolymers act as nucleating agents. The CNW-g-P(LLA-b-CL) induces greater effect.

The PLAs with random end block copolymer show a bimodal endothermic fusion at higher melting temperature (one is at 164°C and other one at 168°C) than neat PLA. The peak at 168°C is attributed by a recrystallization during scanning of heating. ^[9,47]

Table 3.8 DSC data obtained from figure 3.14 regarding PLA, PLA/CNW 100/5, PLA/CNW-g-P(LLA-co-CL) 100/5 and PLA/CNW-g-P(LLA-b-CL) 100/5.

Sample	Second Heating Scan						
	PLA Cold Cryst.		PLA Tg	PLA Melting			
	Tcc (°C)	ΔHcc (J/g)	Tg (°C)	Tm1 (°C)	ΔHm1 (J/g)	Tm2 (°C)	ΔHm2 (J/g)
PLA	129	-27.8	61	166	33.3		
PLA/CNW 100/5	125	-31.7	63	166	37.7		
PLA/CNW-g-P(LLA-co-CL) 100/5	118	-31.4	62	164	32.8	169	8.3
PLA/CNW-g-P(LLA-b-CL) 100/5	109	-26.9	63	162	12.9	168	24.1

The figure 3.15 a) shows the thermal scans of following blends:

- PLA/PCL 80/20;
- PLA/PCL/CNW 80/20/5;
- PLA/PCL/CNW-g-P(LLA-co-CL) 80/20/5;
- PLA/PCL/CNW-g-P(LLA-b-CL) 80/20/5.

In the cooling scan, all blends have the exothermic peaks of the PCL crystallization between 23°C and 33°C.

Indeed, PCL is a highly flexible polyester able to crystallize during rapid cooling.

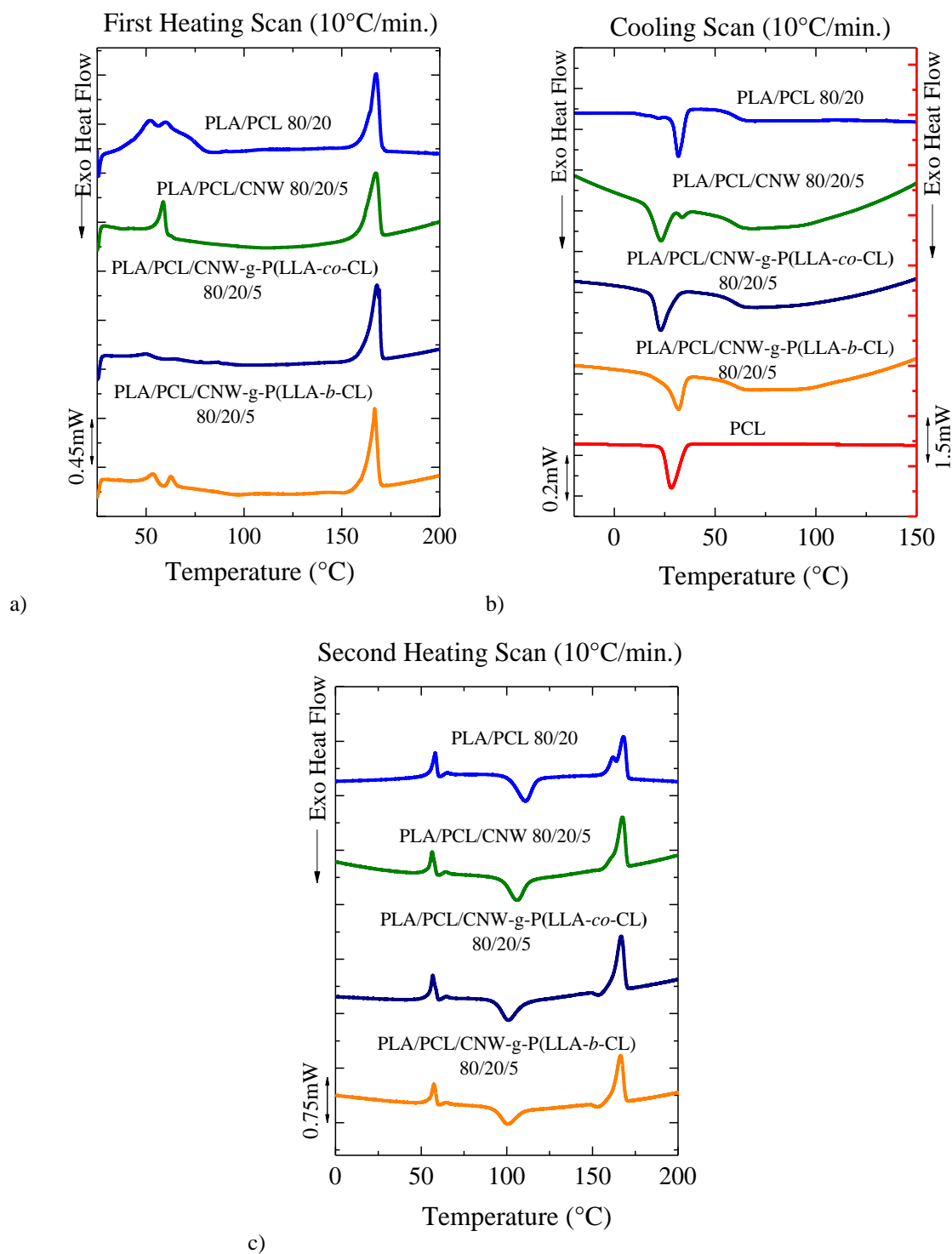


Figure 3.15 a) DSC first heating scan. b) DSC Cooling scan from the melt following the first heating scan shown in a) c) Subsequent DSC second heating scan after the cooling run shown in b) for the PLA/PCL 80/20, PLA/PCL/CNW 80/20/5, PLA/PCL/CNW-g-P(LLA-co-CL) 80/20/5, PLA/PCL/CNW-g-P(LLA-b-CL) 80/20/5 and PCL.

The blends with CNW and CNW-g-P(LLA-co-CL) have a crystallization temperature at 23°C (as shown in table 3.9) while the PLA/PCL 80/20 and blend containing CNW-g-P(LLA-b-CL) has a higher temperature of crystallization at about 32°C.

The lowering of crystallization temperature of PCL is caused by fractionated crystallization. However, the morphology analysis with the scanning electron microscope are indispensable to confirm this behaviour.

Table 3.9 DSC data obtained from figure 3.15 regarding PLA/PCL 80/20, PLA/PCL/CNW 80/20/5, PLA/PCL/CNW-g-P(LLA-co-CL) 80/20/5, PLA/PCL/CNW-g-P(LLA-b-CL) 80/20/5 and PCL

Sample	Cooling Scan				PLA Tg (°C)
	PCL Cryst.				
	Tcc ₁ (°C)	ΔHcc ₁ (J/g)	Tcc ₂ (°C)	ΔHcc ₂ (J/g)	
PLA/PCL 80/20			32	-37,7	57
PLA/PCL/CNW 80/20/5	23	-38,5	34	-2,3	57
PLA/PCL/CNW-g-P(LLA-co-CL) 80/20/5	23	-38,1			58
PLA/PCL/CNW-g-P(LLA-b-CL) 80/20/5			32	-27,3	57
PCL			29	-59,5	

In the second heating scan, a first endothermic peaks between 57 °C and 58 °C are caused by the melting of the crystalline phase of the PCL.

From 100°C to 110°C there is a exothermic peak of the cold crystallization of the PLA. Finally, there is an endothermic peak between 166°C and 168°C, which indicates the crystal melting of PLA.

The presence of the melting peak of polycaprolactone (T_m= 58°C) near glass transition temperature of PLA, prevents an analysis of the possible changes of amorphous PLA phase in blends containing PCL. In them blends, the crystallization temperatures of PLAs have not remarkable changes because the nanofillers don't act as nucleating agents.

This behavior is very difficult to understand. The nucleating agents have a different effect if they stay on the interface between blended polymers or if they stay inside of polymeric matrix.

The PLA/PCL 80/20 blend shows a bimodal endothermic fusion, which is caused by recrystallization of PLA. [9]

Table 3.10 DSC data obtained from Figure 3.15 regarding PLA/PCL 80/20, PLA/PCL/CNW 80/20/5, PLA/PCL/CNW-g-P(LLA-co-CL) 80/20/5, PLA/PCL/CNW-g-P(LLA-b-CL) 80/20/5 and PCL.

Second Heating Scan										
Sample	PCL Melting		PLA ColdCryst.				PLA Melting			
	T _m (°C)	ΔH _m (J/g)	T _{cc1} (°C)	ΔH _{cc1} (J/g)	T _{cc2} (°C)	ΔH _{cc2} (J/g)	T _{m1} (°C)	ΔH _{m1} (J/g)	T _{m2} (°C)	ΔH _{m2} (J/g)
PLA/PCL 80/20	58	36.3	111	-27.9			163	10.2	168	16.6
PLA/PCL/CNW 80/20/5	56	35.2	106	-24.6					168	31.4
PLA/PCL/CNW-g-P(LLA-co-CL) 80/20/5	57	37.9	101	-27.5	153	-1.4			167	32
PLA/PCL/CNW-g-P(LLA-b-CL) 80/20/5	58	27.4	100	-21.2	153	-1.5			166	26.5

3.6 Overall isothermal crystallization rate.

To study the isotherm crystallization, analysis at different temperature from the melt have been performed using the DSC instrument on following blends:

- PLA/CNW 100/5 blend;
- PLA/CNW-g-P(LLA-co-CL) 100/5 blend;
- PLA/CNW-g-P(LLA-b-CL) 100/5 blend.
- PLA/PCL/CNW 80/20/5;
- PLA/PCL/CNW-g-P(LLA-co-CL) 80/20/5;
- PLA/PCL/CNW-g-P(LLA-b-CL) 80/20/5.

The samples were heated prior to the analysis at 200 °C to minimize their thermal history. Figure 3.16 shows an example of DSC scans as a function of time collected during isothermal crystallization at various T_c from a melt state (T_c = constant, t = 30 min). Starting temperatures of ~ 30°C higher than the T_g were selected, in a range of about 50°C. This range is chosen because the crystallization process can extend from about 30°C above the glass transition temperature (T_g) at about 10°C below the melting temperature (T_m).^[34] For all samples, for intermediate temperature an increase of the crystallization rate can be observed.

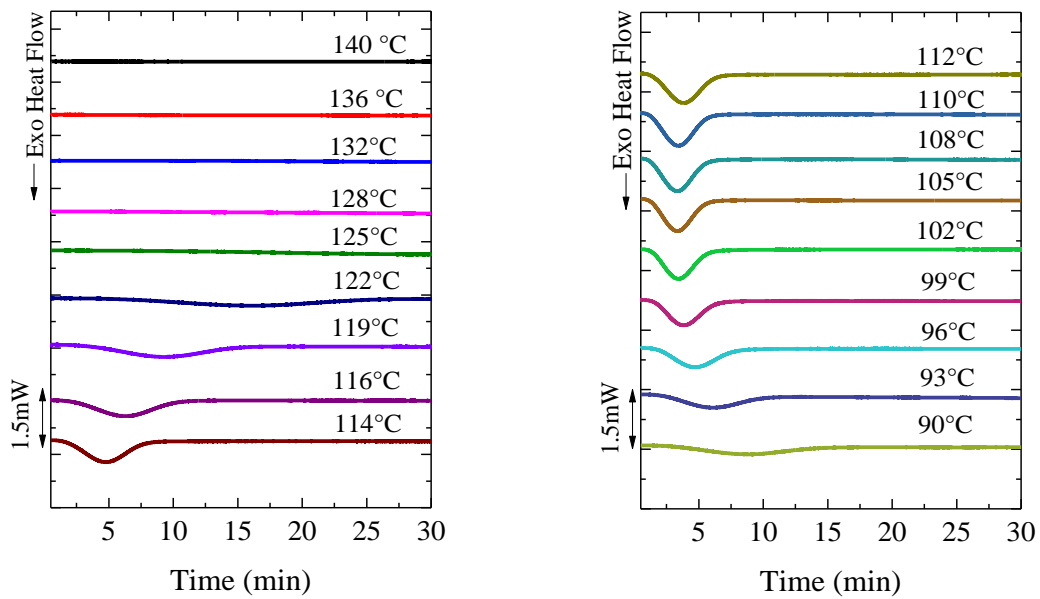


Figure 3.16 Isothermal scans of PLA/PCL/CNW 80/20/5.

The isothermal scans show information on crystallization rate of PLA. For all scans the half-crystallization time, $\tau_{50\%}$, has been calculated, this is the time needed for 50% relative conversion to semi-crystalline state. The inverse overall crystallization rate is proportional to the half-crystallization time.

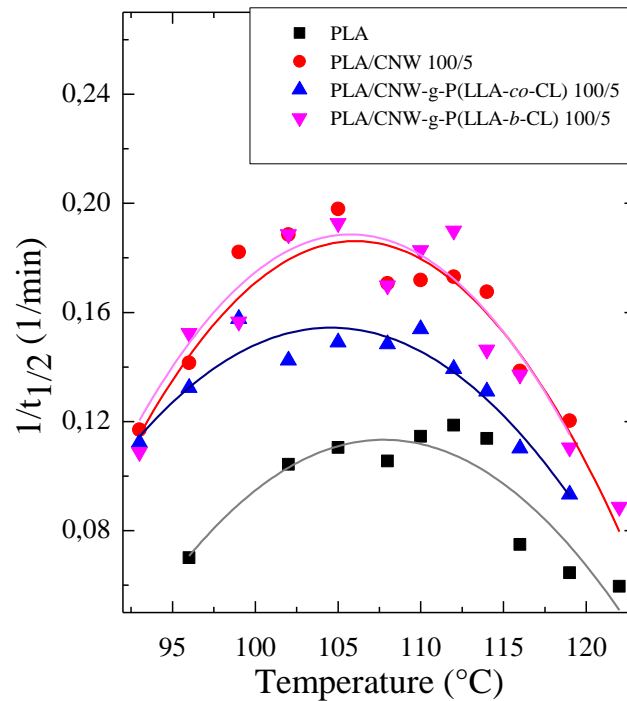


Figure 3.17 Inverse of half-time of crystallization vs. isothermal crystallization temperature for PLA, PLA/CNW 100/5, PLA/CNW-g-P(LLA-co-CL) 100/5 and PLA/CNW-g-P(LLA-b-CL) 100/5.

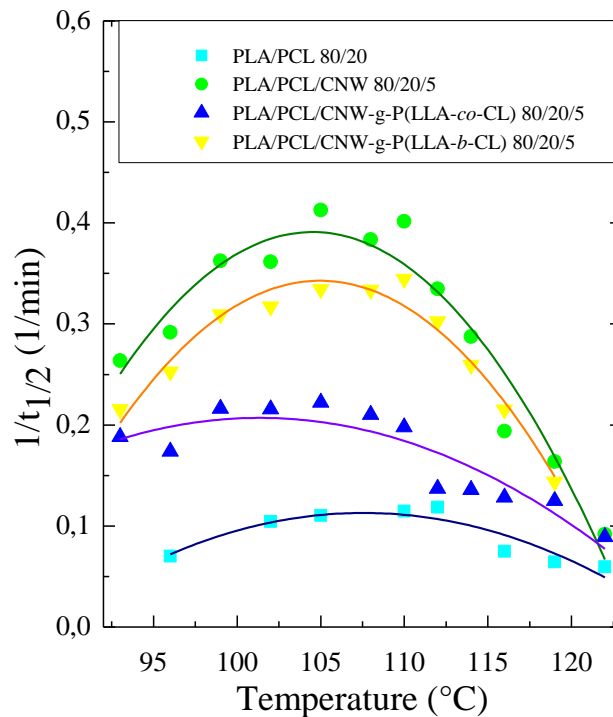


Figure 3.18 Inverse of half-time of crystallization vs. isothermal crystallization temperature for PLA/PCL 80/20, PLA/PCL/CNW 80/20/5, PLA/PCL/CNW-g-P(LLA-co-CL) 80/20/5 and PLA/PCL/CNW-g-P(LLA-b-CL) 80/20/5.

Figure 3.17 shows the trend of crystallization rate with crystallization temperature that includes both the processes of growth and nucleation.

The sample of PLA analysed has stereoregularity of 1.2%- 1.6% D-isomer lactide.

The D-isomer presence causes slow crystallization rate.

The experimental data, represented in the figure 3.17, indicate that the blends with nanofillers show a remarkable reduction of $\tau_{50\%}$ in comparison with neat PLA.

In particular, higher percentage of CNW causes improvement of crystallization rate. Indeed, the neat nanocellulose is a efficient nucleating agent.^[9]

The nanofillers have a different percentage of CNW: 70% in random copolymer while 90% in block copolymer.

The reduced $\tau_{50\%}$ of block copolymers is caused by higher percentage of nanocellulose.

This effect is clearer in the PLA/PCL 80/20 blends, as shown in figure 3.18.

The PLA/PCL 80/20 presents remarkable reduction of the variable $\tau_{50\%}$ compared with neat PLA (about a half of the neat PLA time).

In immiscible PLA/PCL blend, the PCL donate impurities to PLA acting as nucleating agent.

For the analysis of data obtained by DSC under isothermal condition, we used the Avrami's equation. For both blends, in intermediate isotherms, with an interval between of 122°C-119°C and 93°C, a considerable increase in the rate of crystallization occurs allowing the application of Avrami's equation.

According to Avrami, the progress of the isothermal crystallization can be expressed by the equation: ^[34]

$$1-V_c = \exp(-k(t-t_0)^n) \quad \text{Equation 3.2}$$

Where V_c is the crystalline volume fraction, k is the constant rate of the overall crystallization, t_0 is the induction time, n is the Avrami index that assumes different values depending on the type of geometry of crystal growth and the type of nucleation. Applying the logarithmic properties on both sides of the equation 3.2, the following equation can be obtained:

$$\log[-\ln(1 - V_c)] = \log(k) + n \log(t - t_0) \quad \text{Equation 3.3}$$

This equation is called Avrami linear equation. Plotting $\log[-\ln(1 - V_c)]$ as a function of $\log(t - t_0)$ the values of k and n can be obtained. A very important value in the Avrami's theory is the time required by the material to reach the half-crystallization time and can be indicated as $\tau_{1/2}$ or $\tau_{50\%}$. It is possible to calculate it through this equation: ^[34]

$$\tau_{1/2} = \left(\frac{-\ln(1-V_c)}{k} \right)^{1/n} = \left(\frac{-\ln(0.5)}{k} \right)^{1/n} \quad \text{Equation 3.4}$$

The inverse of the half-crystallization time is proportional to the overall crystallization rate. Conversion of the semicrystalline state from 3% to 20% was used for all the samples; the conversion values lower than 3% fall within equipment errors, while those exceeding 20% have shown a deviation between the theoretical and the experimental data. ^[48]

The following figure 3.19 show a example of the analysed isothermal curves obtained applying the theory of Avrami. Figure 3.19 a) is the graph of the Avrami linear equation where it is possible to calculate the Avrami index, n , which is the slope of the line and the rate constant, K , which is the y-intercept; figure 3.19 b) shows the relationship between the semi-logarithmic amorphous fraction and the material $(1 - V_c)$ and $\log(t - t_0)$; figure 3.19 c) shows the graphs for the theoretical and experimental isothermal crystallization process; figure 3.19 d), the last graph, indicates the change of the enthalpy of crystallization as a function of crystallization time; from this curve we can obtain the value of $\tau_{50\%}$ ^[48]

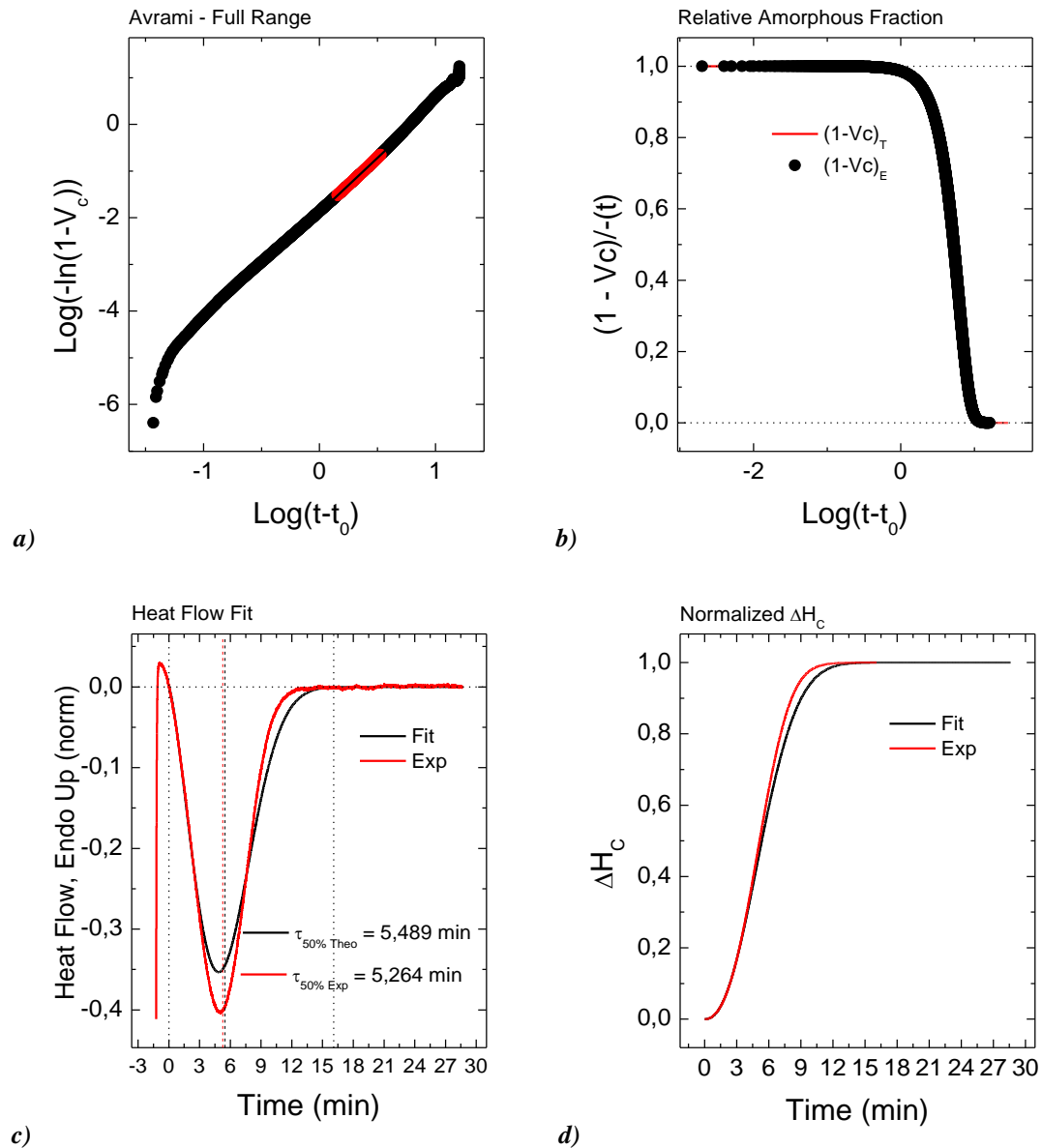


Figure 3.19 a) Avrami plot. b) Unconverted relative volumetric fraction as a function of time for the isothermal crystallization of the PLA at 112°C. Comparison between the experimental data and Avrami fit. c) Comparison between experimental DSC isothermal and Avrami prediction for PLA isothermally crystallized at 10°C. d) change of the enthalpy of crystallization as a function of crystallization time.

The following table 3.11 shows the Avrami's indexes n , the constant of overall crystallization k^{-n} , experimental $\tau_{1/2exp}$, theoretical $\tau_{1/2theo}$, (which for both indicates the time required to obtain 50% of the conversion of increase, the crystalline state), and the linearity error R^2 .

It is important to know these data in order to compare the crystallization rates of the different blends.

Table 3.11 Data obtained by the Avrami model

Sample	T _c (°C)	n	k ⁻ⁿ (min ⁻ⁿ)	τ _{1/2} ^{Theo} (min)	τ _{1/2} ^{Exp} (min)	R ²
PLA	122	2.38	0.0007	17.602	16.767	1
	119	2.25	0.0013	16.051	15.492	1
	116	2.02	0.0032	14.440	13.335	1
	114	1.79	0.0109	10.125	8.788	0,9996
	112	1.72	0.0135	9.839	8.430	0.9996
	110	1.7	0.0132	10.260	8.727	0.9995
	108	1.7	0.0116	11.075	9.475	0.9995
	105	1.79	0.0103	10.514	9.050	0.9991
	102	1.75	0.0102	11.208	9.582	0.9991
	99	/	/	/	/	/
96	2.02	0.0027	15.513	14.267	0.9992	
PLA/CNW 100/5	119	2.05	0.0084	8.648	8.310	1
	116	2.17	0.0089	7.471	7.217	1
	114	2.05	0.0156	6.365	5.969	0.9999
	112	2.1	0.0153	6.150	5.777	0.9997
	110	2.22	0.0123	6.146	5.817	0.9998
	108	2.25	0.0115	6.175	5.860	0.9998
	105	2.17	0.0190	5.241	5.052	0.9999
	102	2.18	0.0168	5.488	5.305	0.9999
	99	2.08	0.0187	5.675	5.492	1
	96	2.08	0.0112	7.271	7.065	1
93	2.06	0.0077	8.816	8.547	1	
PLA/CNW-g-P(LLA-co-CL) 100/5	119	3.08	0.0005	10.719	10.721	1
	116	2.88	0.0012	9.135	9.080	1
	114	2.48	0.0043	7.776	7.630	1
	112	2.29	0,0067	7.606	7.180	0.9998
	110	2.01	0.0130	7.254	6.497	0.9994
	108	2.05	0.0113	7.456	6.743	0.9993
	105	2.04	0.0140	7.745	6.712	0.9991
	102	2.16	0.0085	7.643	7.022	0.9996
	99	2.42	0.0074	6.549	6.342	0.9999
	96	2.43	0.0046	7.822	7.556	0.9999
93	2.37	0.0036	9.212	8.906	0.9999	
PLA/CNW-g-P(LLA-b-CL) 100/5	122	3.02	0.0005	11.081	11.265	1
	119	2.83	0.0014	9.048	9.048	1
	116	2.61	0.0038	7.342	7.288	1

	114	2.74	0.0034	6.935	6.830	1
	112	2.34	0.0130	5.489	5.264	0.9999
	110	2.23	0.0140	5.737	5.470	0.9998
	108	2.5	0.0080	5.977	5.886	1
	105	2.41	0.0126	5.282	5.190	1
	102	2.57	0.0095	5.309	5.301	0.9999
	99	2.71	0.0045	6.418	6.384	1
	96	2.18	0.0104	6.888	6.561	0.9999
	93	2.2	0.0048	9.562	9.187	0.9999
	122	2.39	0.0020	11.482	10.902	0.9998
	119	2.32	0.0009	6.388	6.105	0.9999
	116	2.77	0.0068	5.313	5.157	0.9999
	114	2.5	0.0278	3.613	3.478	0.9998
	112	2.56	0.0424	2.983	2.988	0.9998
PLA/PCL/CNW 80/20/5	110	2.45	0.0683	2.570	2.490	0.9999
	108	2.65	0.0527	2.642	2.607	1
	105	2.55	0.0686	2.474	2.422	0.9999
	102	2.94	0.0351	2.759	2.766	1
	99	2.59	0.0486	2.795	2.758	1
	96	2.54	0.0288	3.495	3.428	0.9999
	93	2.23	0.0331	3.922	3.792	0.9999
	122	2.35	0.0022	11.636	11.214	0.9999
	119	2.16	0.0071	8.312	8.013	0.9999
	116	2.2	0.0070	8.082	7.800	0.9999
	114	2.3	0.0062	7.774	7.365	0.9998
	112	2.63	0.0033	7.582	7.297	0.9999
PLA/PCL/CNW-g-P(LLA-co-CL) 80/20/5	110	2.26	0.0016	5.253	5.053	0.9999
	108	2.24	0.0191	4.956	4.759	0.9999
	105	2.2	0.0235	4.670	4.498	0.9999
	102	2.21	0.0212	4.854	4.636	0.9998
	99	2.16	0.0234	4.789	4.624	0.9999
	96	2.17	0.0141	5.991	5.760	0.9999
	119	2.88	0.0027	6.909	6.947	1
	116	2.36	0.0174	4.754	4.645	1
	114	2.31	0.0294	3.924	3.854	1
	112	2.28	0.0436	3.367	3.304	1
PLA/PCL/CNW-g-P(LLA-b-CL) 80/20/5	110	2.21	0.0606	3.007	2.901	1
	108	2.28	0.0555	3.027	2.994	1
	105	2.29	0.0510	3.119	2.990	1
	102	2.44	0.0398	3.234	3.152	1

99	2.33	0.0423	3.316	3.230	1
96	2.33	0.0260	4.101	3.953	1
93	2.19	0.0212	4.915	4.639	0.9998

Avrami's index depends on the size of the crystals and the type of nucleation.

If the crystallization is instantaneous the Avrami index will be between 1 and 3, where $n = 1$ is a cylindrical morphology (one dimensional), $n = 2$ is a disc structure (two dimensional), $n = 3$ is a spherical structure (three dimensional).^[34]

The sporadic crystallization is characterized by the increase in unit of n for each of the dimensions, however it is very unusual to obtain an integer value.

As the table 3.11 and in figures 3.20 and 3.21 clearly shows the Avrami index changes according to the samples: for PLA and PLA/CNW 100/5, $n = 1.7-2.5$, indicating an instantaneous two-dimensional increase; for PLA/CNW-g-P(LLA-co-CL), PLA/CNW-g-P(LLA-b-CL) 100/5 and PLA/PCL/CNW 80/20/5 $n = 2.39-3.04$ indicating an instantaneous three-dimensional, with finally PLA/PCL/CNW-g-P(LLA-co-CL) and PLA/PCL/CNW-g-P(LLA-b-CL) 80/20/5 $n = 2.19-2.65$ indicating an immediate two-dimensional increase.

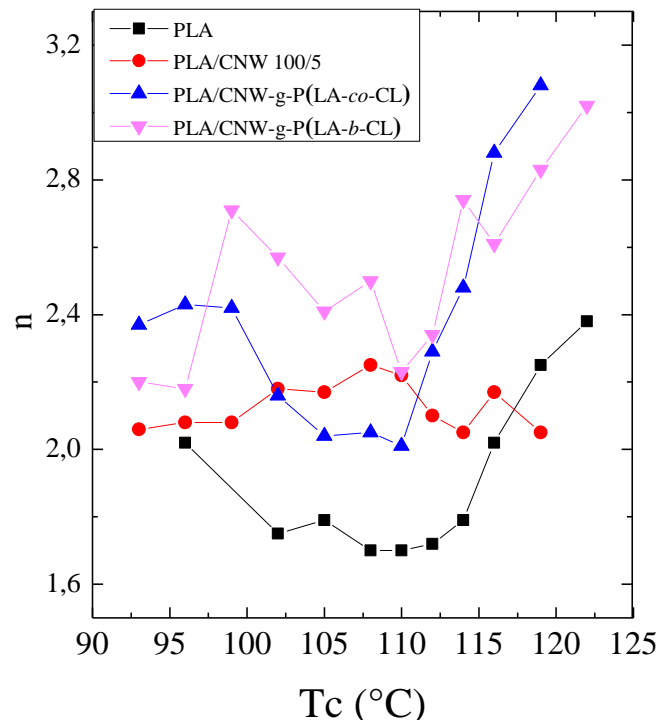


Figure 3.20 Variation of Avrami's index with T_c for PLA, PLA/CNW 100/5, PLA/CNW-g-P(LLA-co-CL) 100/5 and PLA/CNW-g-P(LLA-b-CL) 100/5.

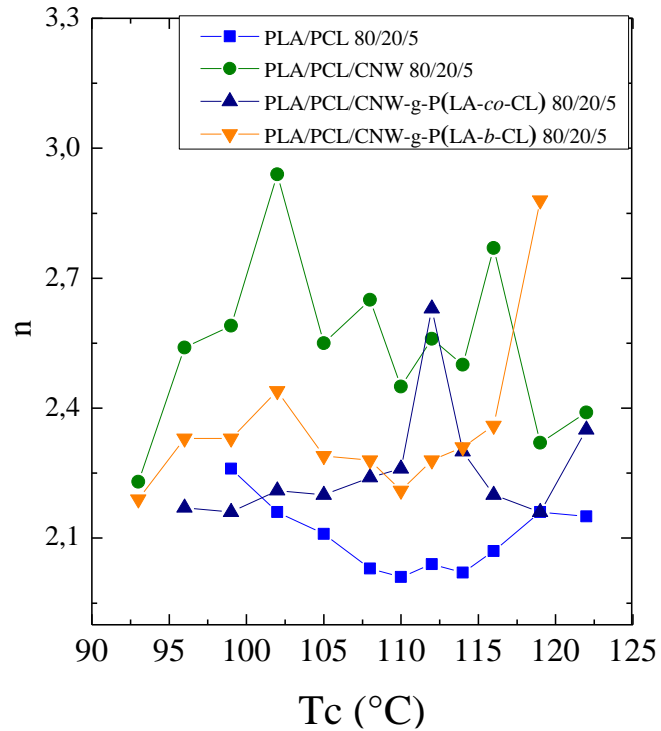


Figure 3.21 Variation of Avrami's index with Tc for PLA/PCL 80/20, PLA/PCL/CNW 80/20/5, PLA/PCL/CNW-g-P(LLA-co-CL) 80/20/5 and PLA/PCL/CNW-g-P(LLA-b-CL) 80/20/5.

The constant of overall crystallization k^{-n} has as unit of measure $[\text{min}]^{-n}$, as shown in table 3.11 and it depend on Avrami index. In order to eliminate this dependence, k^{-n} has been normalized, in k, raising $1/n$, $(\text{min}^{-n})^{1/n}$.

Moreover the k^{-n} normalization, allow to avoid error to compare the parameters. Figures 3.22 and 3.23 show the variation of k values as function of crystallization temperature. The trend in this parameter is related with that in the crystallization rate.

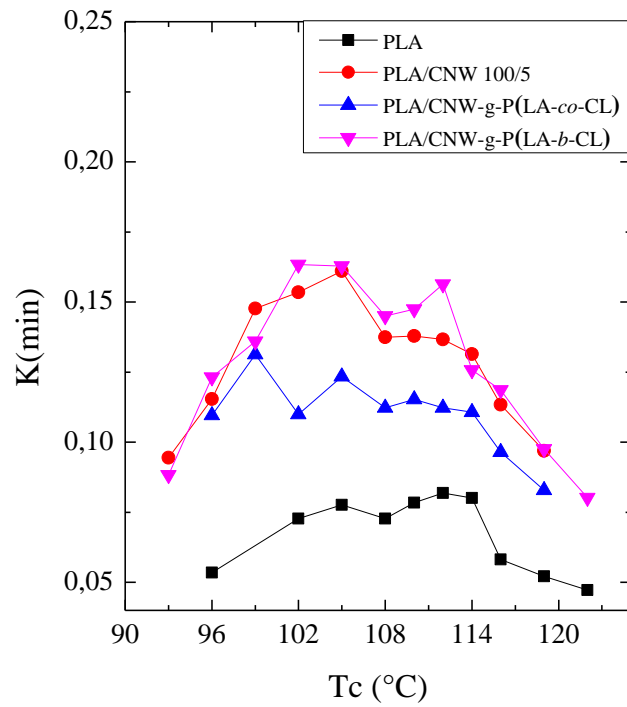


Figure 3.22 Variation of k values with Tc for PLA, PLA/CNW 100/5, PLA/CNW-g-P(LLA-co-CL) 100/5 and PLA/CNW-g-P(LLA-b-CL) 100/5.

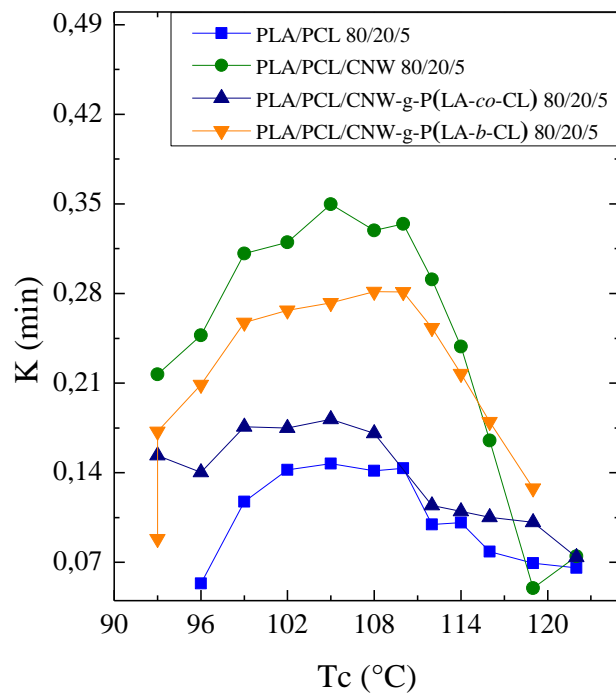


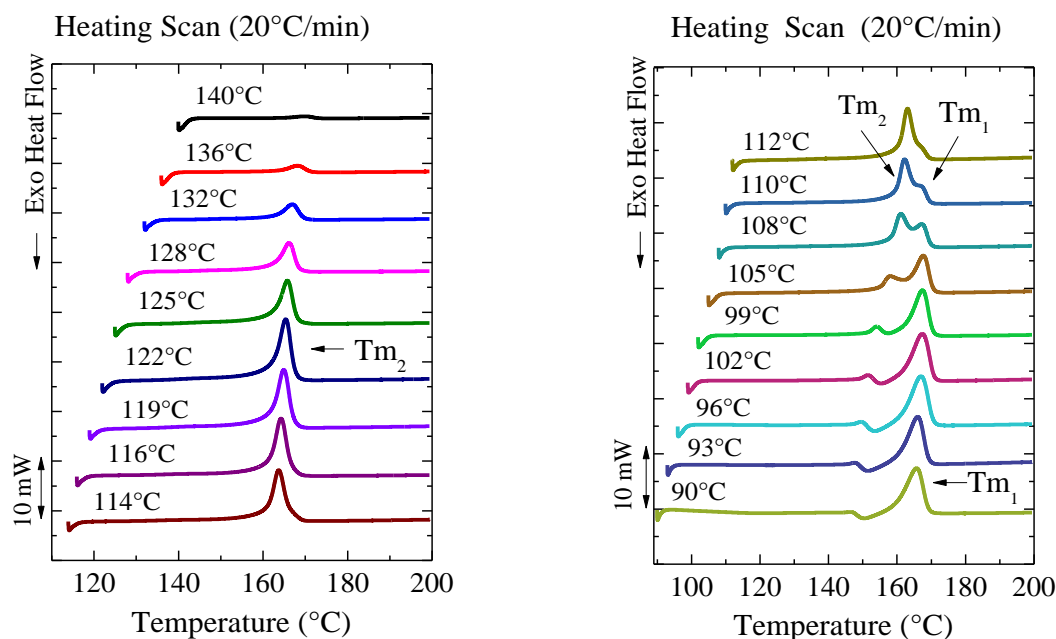
Figure 3.23 Variation of k values with Tc for PLA/PCL 80/20, PLA/PCL/CNW 80/20/5, PLA/PCL/CNW-g-P(LLA-co-CL) 80/20/5 and PLA/PCL/CNW-g-P(LLA-b-CL) 80/20/5.

After the Avrami equation the theory of Lauritzen and Hoffman was used, this allows to determine parameters such as the energy barrier for growth and nucleation (K_g^τ), the folding surface free energy (σ_e) and the work required to make a bend (q).

For the application of this model, we need to calculate the value of the temperature at the melting equilibrium (T_m^0) through the Hoffmann-Weeks method.^[51]

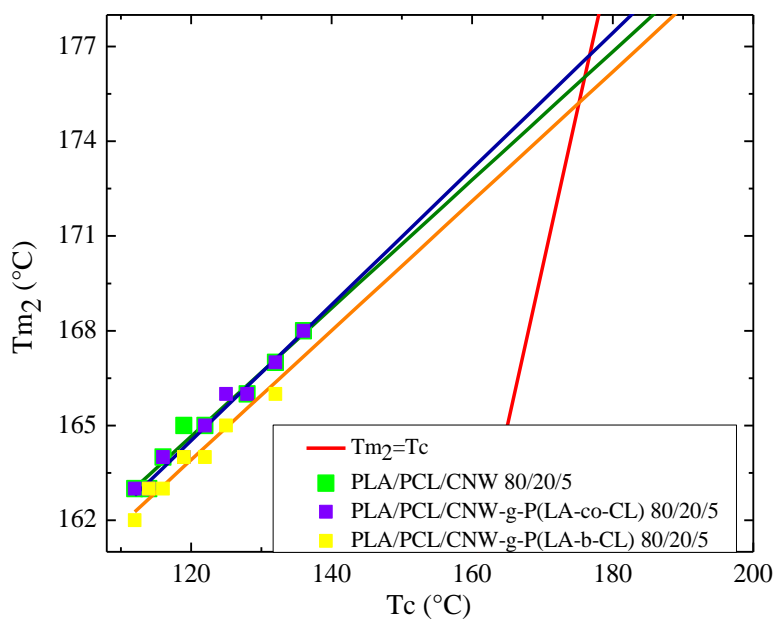
The T_m^0 is experimentally extrapolated by observing its melting points of the heating scans of each sample.

Figure 3.24 a) and b) shows an example of heating scans (at a rate of 20 °C/min) performed after isothermal crystallization. Two melting peaks stand out indicated by the arrows: first melting temperature (T_{m1}) and second melting temperature (T_{m2}). Plotting the T_{m2} vs T_c and the line $T_m = T_c$, the value of T_{m0} was obtained from the point of intersection of them. (As shown in figure 3.24 c))



a)

b)



c)

Figure 3.24 DSC heating scans for a) b) PLA/PCL/CNW 80/20/5, with a heating rate of 20°C/min after isothermal crystallization at various temperatures T_c . c) Variation of T_{m2} with T_c for PLA/PCL/CNW 80/20/5, PLA/PCL/CNW-g-P(LLA-co-CL) 80/20/5 and PLA/PCL/CNW-g-P(LLA-b-CL) 80/20/5.

The T_{m0} values fall in the range of 174°C- 177°C, as shown in the figure 3.24 c).

Studies undertaken by Huang et al [49] show that the existence of double-melting peaks in the curves of the isothermal heating is derived by the polymorphic nature of the PLA; due to the presence of two crystalline structures, with different thicknesses of the the crystal lamellae.

T_{m1} is the result of the melting of the crystallites recrystallized during the heating process, while the lower melting peak T_{m2} refers to the melting of the primary crystallites formed during the isothermal crystallization process.

Knowing the T_{m0} and the data of isothermal crystallization rate it is possible to apply the equation of Lauritzen-Hoffman in order to compare the variations between the experimental and theoretical data of the overall crystallization rate ($1/\tau_{1/2}$ vs T_c) and the closeness of the values obtained by the two methods.

Figures 3.25, 3.26, 3.27 and 3.28 show the trend of the linear crystallization rate in relation to the supercooling degree for all the samples.

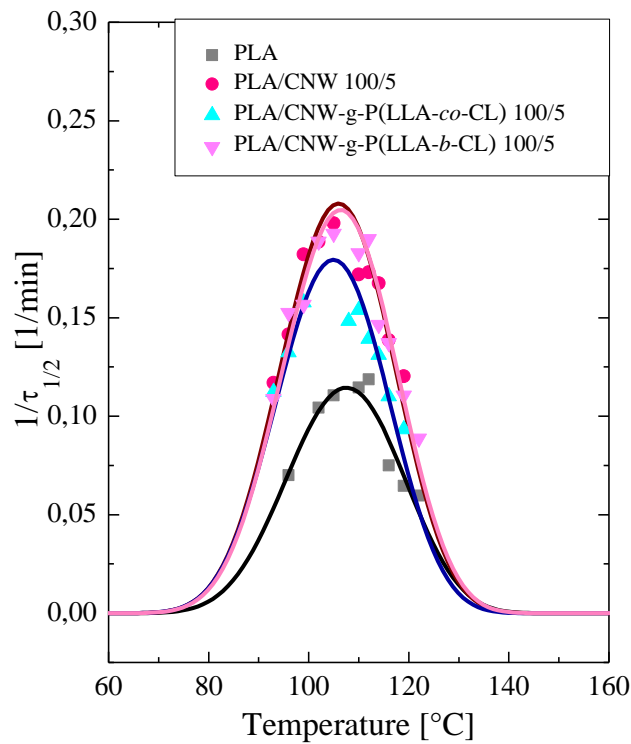


Figure 3.25 Plots of $1/\tau_{1/2}$ as a function T_c of PLA, PLA/CNW 100/5, PLA/CNW-g-P(LLA-co-CL) 100/5 and PLA/CNW-g-P(LLA-b-CL) 100/5.

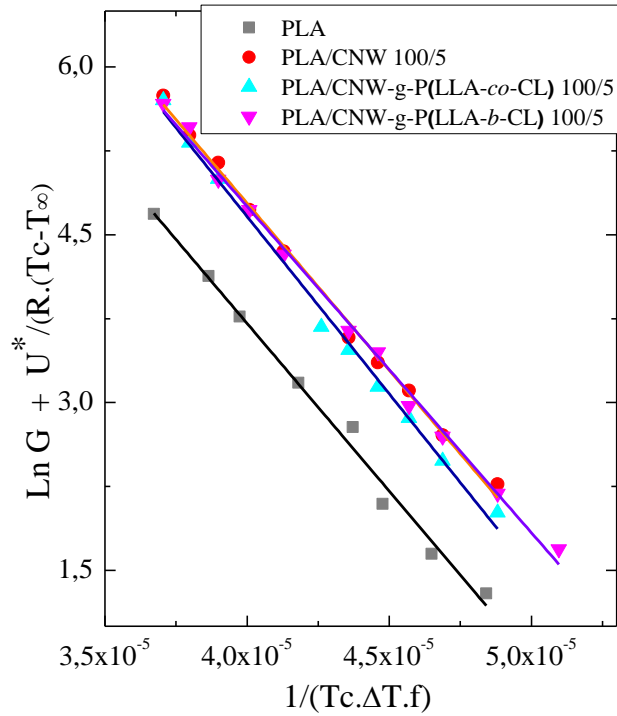


Figure 3.26 Plots of $\ln G + U^*/R(T_c - T_\infty)$ as a function $1/T_c \Delta T f$ of the PLA, PLA/CNW 100/5, PLA/CNW-g-P(LLA-co-CL) 100/5 and PLA/CNW-g-P(LLA-b-CL) 100/5.

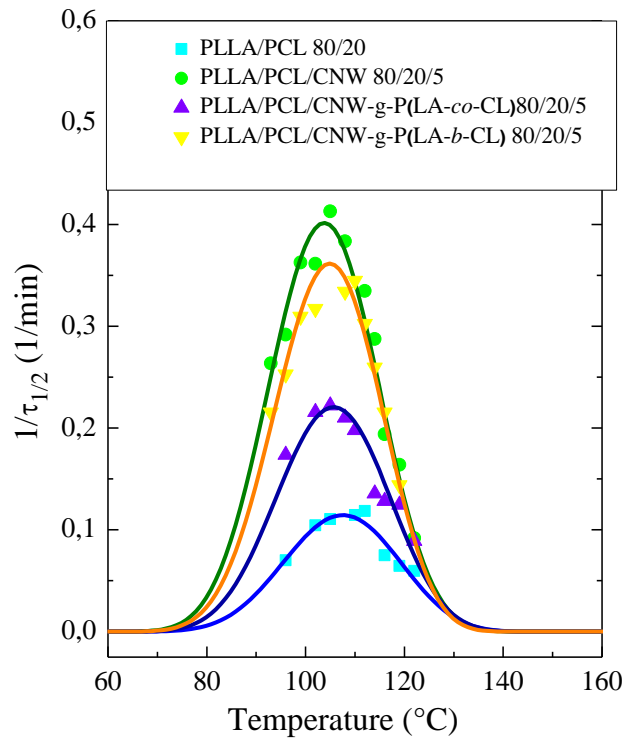


Figure 3.27 Plots of $1/\tau_{1/2}$ as a function T_c data of PLA/PCL 80/20, PLA/PCL/CNW 80/20/5, PLA/PCL/CNW-g-P(LLA-co-CL) 80/20/5 and PLA/PCL/CNW-g-P(LLA-b-CL) 80/20/5.

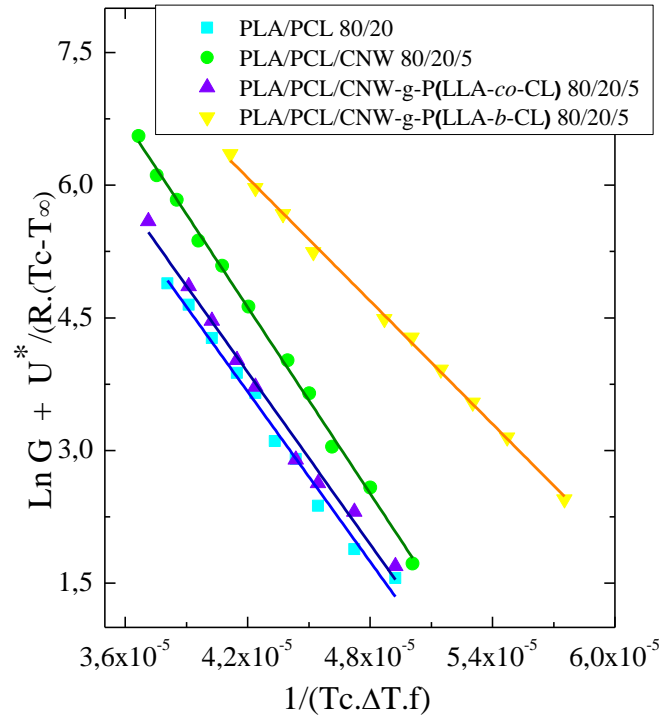


Figure 3.28 Plots of $\ln G + U^*/R(T_c - T_\infty)$ as a function $1/T_c \Delta T f$ of the PLA/PCL 80/20, PLA/PCL/CNW 80/20/5, PLA/PCL/CNW-g-P(LLA-co-CL) 80/20/5 and PLA/PCL/CNW-g-P(LLA-b-CL) 80/20/5.

In figure 3.25 and 3.27, the bell-shaped trends of experimental data can be observed as well as theoretical values represented by the continuous lines. The temperature range in which to observe this behaviour is bounded by two values: the T_g and the T_m . At temperatures near to the melting, crystallization rate is very low and the process is controlled by the nucleation, which is hindered at high temperatures. Lowering the temperature, the crystallization rate increases gradually and returns to decrease when the crystallization is controlled by diffusion, which is hindered at low temperature.

In all samples we have several very close data points which of course fit a straight line in the L-H plot (Figures 3.26 and 3.28)

Table 3.12 shows the values obtained in terms of energy barrier of nucleation and growth crystal increase (K^t_g), σ_e indicates the free energy of folding, σ is the lateral surface free energy, q the work necessary to achieve a bending, the pre-exponential factor is A^0 and the linearity error is R^2 .

Table 3.12 Data obtained using the model L-H with DSC

Sample	K_g^{τ} (II) (K²)	σ (erg/cm²)	σ_e (erg/cm²)	q (erg)	R²
PLA	3.00 E+05	8.08	260.55	9.61 E-13	0.9909
PLA/CNW 100/0/5	2.99 E+05	8.08	261.32	9.64 E-13	0.9963
PLA/CNW-g-P(LLA-co-CL) 100/5	3.17 E+05	8.08	277.29	1.02E-12	0.9953
PLA/CNW-g-P(LLA-b-CL) 100/5	2.92 E+05	8.08	255.11	9.41 E-13	0.9964
PLA/PCL 80/20	2.29 E+05	8.08	278.68	1.03 E-12	0.9894
PLA/PCL/CNW 80/20/5	3.50 E+05	8.08	305.73	1.13 E-12	0.9969
PLA/PCL/CNW-g-P(LLA-co-CL) 80/20/5	3.31 E+05	8.08	288.15	1.06 E-12	0.9845
PLA/PCL/CNW-g-P(LLA-b-CL) 80/20/5	3.11 E+05	8.08	272.36	1.01 E-12	0.9982

4. CONCLUSIONS

In this thesis several experimental techniques were employed to characterize the random poly(L-lactide-*co*- ϵ -caprolactone) and the block poly(L-lactide-*b*- ϵ -caprolactone) grafted on cellulose nanowhiskers, CNW-g-P(LLA-*co*-CL) and CNW-g-P(LLA-*b*-CL), and to study of the overall crystallization rate of PLA phase in the neat PLA and PLA/PCL 80/20 blend eventually added with synthesized nanofillers and neat cellulose nanowhiskers (CNW).

The following conclusions can be derived from the analysis of the results obtained on the random and block copolymers:

- The nuclear magnetic resonance ($^1\text{H-NMR}$) analysis demonstrated that:

1. in the reaction in toluene the composition of copolymer is different from the feed composition at 85°C; while the reaction in xylene and in bulk at 120°C have the correct composition of the grafted chains.
2. The effective formation of block copolymer.

-Attenuated total reflection infrared analysis (ATR-IR) confirmed the successful grafting in all reaction. The ATR-IR spectrum shows that the grafting of the reaction in bulk is not efficient. This fact can be attributed to a reduction of the nanocellulose dispersion due to the high viscosity.

-Thermal gravimetric analysis (TGA) demonstrated that the random copolymers in bulk have a low percentage of grafted polymer (this confirm the difficulty of the reaction media to polymerize) and a greater thermal instability when the amount of the catalyst increases. TGA analysis show that the nanofillers have a different percentage of CNW: random copolymer has 70% while block has 90%.

-Differential scanning calorimetry (DSC) non-isothermic analysis shown peaks of the crystallization of PLA and PCL phases within block copolymer. In random copolymer a crystalline phase is not present because of random distribution at leasy for the used composition (50% mol of LA and 50% mol of PCL).

The following conclusions can be derived from the analysis of the results obtained on neat PLA and PLA/PCL 80/20 blend with nanofillers:

- TGA displayed a faster rapid degradation in the blend containing CNW-g-P(LLA-*co*-CL) and CNW-g-P(LLA-*b*-CL) than other ones. This behaviour may be caused by the fact that grafted copolymers have a lower packing rate compared to that of nanocellulose.

-DSC non-isothermic in the second heating scan of neat PLA with nanofillers show that:

1. All blends exhibited slow cold crystallization behaviour because of the presence of only 1.2% of D-isomer in the PLA matrix.
2. Lowering of crystallization temperature indicates that random and block copolymer act as nucleating agents. The CNW-g-P(LLA-*b*-CL) induces greater effect.
3. PLA/CNW-g-P(LLA-*co*-CL) 100/5 and PLA/CNW-g-P(LLA-*b*-CL) 100/5 blends shown a bimodal endothermic fusion, which is caused by a recrystallization during heating scan.

-DSC non-isothermic analysis on PLA/PCL 80/20 blends with nanofillers has highlighted that the crystallization temperatures of PLA have not remarkable changes. The nanofillers don't act as nucleating agents. This phenomenon is very difficult to understand. The nucleating agents may have different effect depending on position in the polymer matrix.

-DSC isothermal analysis demonstrate that all blends containing nanofillers had a remarkable increasing of PLA crystallization rate compared to neat blends, especially in presence of nanocellulose. In particular, high percentage of CNW causes improvement of crystallization rate.

5. EXPERIMENTAL SECTION

5.1 Materials.

The cellulose nanowhiskers (kindly provided by Prof. Alejandro J. Müller's laboratory) has been used. The L-lactide (Sigma-Aldrich-CAS Number: 4511-42-6) has been previously purified by recrystallization from boiling toluene, and following complete elimination of solvent under vacuum for 3 hours. The ϵ -caprolactone (Sigma-Aldrich-CAS Number: 502-44-3) was purified by vacuum distillation. Tin(II)octoate (Sigma-Aldrich-CAS Number: 301-10-0) was used as catalyst. A mixture of xylene isomers (Sigma-Aldrich-CAS Number: 1330-20-7), previously dried on sodium sulfate, was used as solvent. Toluene (Sigma-Aldrich-CAS Number: 108-88-3), which was purified by simple distillation, was used as solvent. The polymers used for blends are: poly(ϵ -caprolactone) (molar mass 80000 g/mol) supplied by Solvay, poly(lactide) (trade name 4032D, Nature Works) with high stereoregularity (1.2%-1.6% D-isomer lactide). All the used glassware was dried in an oven at 105 °C for at least 4 hours.

5.2 Synthesis in bulk of random co-polymer lactide and ϵ -caprolactone grafted on cellulose (CNW-g-P(LLA-co-CL)).

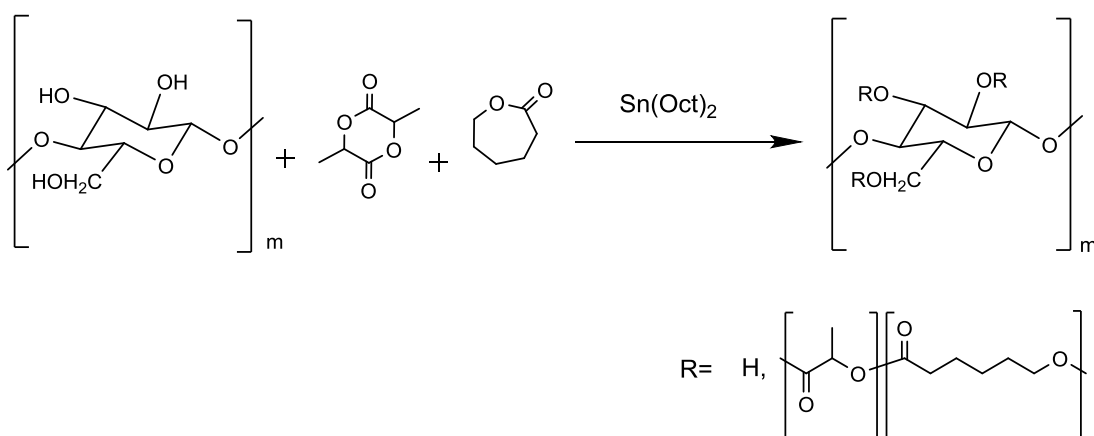


Figure 5.1 Synthesis of random copolymer lactide and ϵ -caprolactone grafted on cellulose (CNW-g-P(LLA-co-CL)).

Nanocellulose, lactide and ϵ -caprolactone were added sequentially into a three-neck round-bottom flask containing a magnetic stirrer. The system was kept under nitrogen flow and the flask connected to the column condenser equipped with a calcium chloride (CaCl_2) septum in the head. When a complete dissolution of monomers was achieved tin(II) octoate catalyst was added.

The mixture was put under stirring in an oil bath of 120°C for 48 hours, taking care to ensure that the stirring was always effective. At the end of the reaction the flask was cooled in an ice bath and the crude product (grayish white color) was diluted with a small amount of dichloromethane to reduce viscosity.

To purify the grafted polymer from the presence of non-grafted, the solution was centrifuged for 30 minutes at 3000 rpm, whereby the non-grafted part remains in the supernatant. The grafted polymer was placed in a vial and the residual solvent was eliminated under vacuum. The non-grafted polymer was precipitated from the supernatant using a 5-fold volume excess of methanol as non-solvent, thus clearing the polymer from the presence of monomers or oligomers with low molecular weight. The precipitate was placed in a separate vial and the residual solvent was removed in a vacuum.

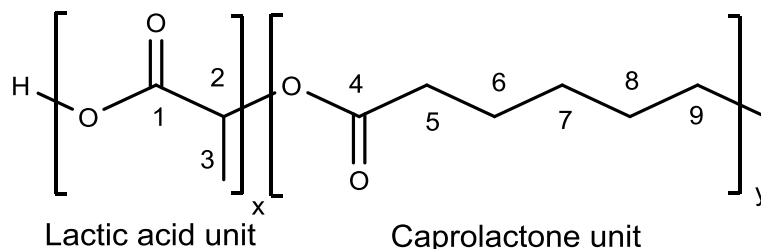


Figure 5.2 Structure of random copolymer lactide and ϵ -caprolactone (P(LLA-*co*-CL)).

$^1\text{H-NMR}$ analysis of the copolymers:

- 1 H of CH (2) at 5.12 ppm
- 3 H of CH_3 (3) at 1.37 ppm
- 2 H of CH_2 (5) at 4.08 ppm
- 6 H of CH_2 (6,7,8) at 1.61 ppm
- 2 H of CH_2 (9) at 2.34 ppm

ATR-IR spectroscopy analysis of the copolymers:

- C = O stretching of the carbonyl groups at about 1734 cm^{-1}
- O-H stretching alcohol of the cellulose at about 3322 cm^{-1}

5.3 Synthesis in bulk of random co-polymer lactide and ϵ -caprolactone grafted on cellulose (CNW-g-P(LLA-co-CL)).

A vial containing a magnetic stirrer was kept under nitrogen flow. Nanocellulose, lactide, ϵ -caprolactone and xylene (or toluene) were added sequentially. The solution was homogenized in an ultrasound for two hours. When a complete dissolution of monomers was achieved tin(II) octoate catalyst was added.

The vial was put under stirring in an oil bath at 120°C (for xylene) or at 85°C (for toluene), taking care to ensure that the stirring is always effective.

At the end of the reaction the vial was cooled in an ice bath and the crude of reaction (straw-yellow color) well dissolved in dichloromethane.

There is the change of color in xylene reaction at different concentrations of catalyst. The color intensity increases by increasing the catalyst. The same purification of paragraph 5.2 has been used for polymer; the only difference is that used a different non-solvent (hexane).

5.4 Synthesis in solution of block copolymer lactide and ϵ -caprolactone grafted on cellulose (CNW-g-P(LLA-*b*-CL)).

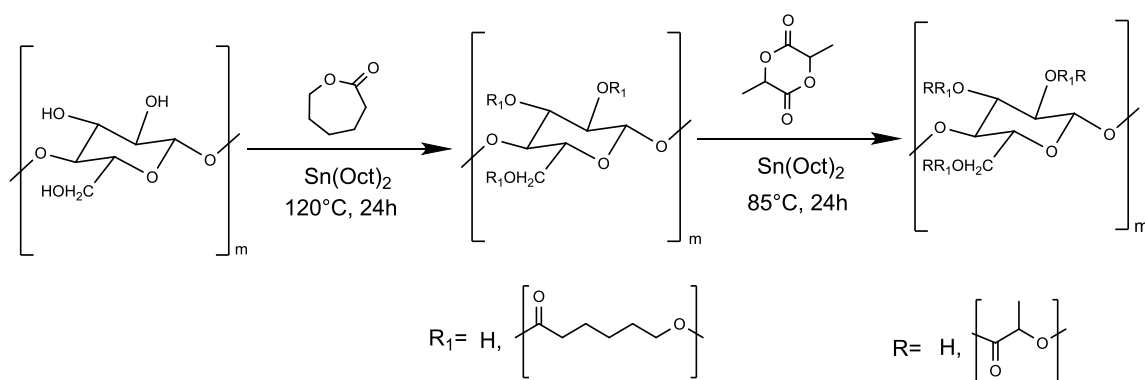


Figure 5.3 Synthesis of block co-polymer lactide and ϵ -caprolactone grafted on cellulose (CNW-g-P(LLA-*b*-CL)).

In a vial containing a magnetic stirrer, under nitrogen flow nanocellulose, ϵ -caprolactone and xylene are placed sequentially. The solution was homogenized in an ultrasound for two hours. When a complete dissolution of monomers was achieved tin(II) octoate catalyst was added.

The vial is put under stirring in an oil bath at 120°C, taking care to ensure that the stirring is always effective. After 24 hours the temperature is lowered to 85 °C, the lactide and

subsequently the same amount of catalyst are added under nitrogen. The same purification of paragraph 5.3 has been used for polymer.

Table 5.1 Summary of the synthesis of the copolymers CNW-g-P(LLA-*co*-CL) and CNW-g-P(LLA-*b*-CL).

Sample	Time(h)	Temp.(°C)	LLA/CL	(LLA+CL)/(Sn(oct) ₂)	OH/Sn(oct) ₂	Solvent
CNW-g-P(LLA- <i>co</i> -CL) 1	48	120	1	150	2	/
CNW-g-P(LLA- <i>co</i> -CL) 2	16.5	120	1	413	1	/
CNW-g-P(LLA- <i>co</i> -CL) 3	16.5	85	1	413	8	toluene
CNW-g-P(LLA- <i>co</i> -CL) 4	48	85	1	36	0.5	toluene
CNW-g-P(LLA- <i>co</i> -CL) 5	48	85	1	72	1	toluene
CNW-g-P(LLA- <i>co</i> -CL) 6	48	120	1	72	0.9	xylene
CNW-g-P(LLA- <i>co</i> -CL) 7	48	120	1	403	5.6	xylene
CNW-g-P(LLA- <i>b</i> -CL) 8	48	120-85	1	106	1.5	xylene

5.5 Preparation of the blends.

In 100 mL flask the preparation of the blend was carried out through the solubilization of neat PLA and neat PCL, then it was added grafted copolymer (CNW-g-P(LLA-*co*-CL) or CNW-g-P(LLA-*b*-CL)) or nanocellulose (table 5.2 shows polymer ratios used) in a suspension in dichloromethane with a polymer concentration 1g/dL, and following to 10 minutes in an ultrasound bath to homogenize. After mixing, in order to remove the solvent, the solution has been left at room temperature for 24 hours, then the residue has been dried under vacuum (60°C for 24 h).

Table 5.2 Composition of blends

Sample	Nanocomposite weight (g)	PLA weight (g)	PCL weight (g)
PLA/PCL/CNW 100/0/5	0.05	1.00	0
PLA/PCL/CNW-g-P(LLA- <i>co</i> -CL) 100/0/5	0.05	1.00	0
PLA/PCL/CNW-g-P(LLA- <i>b</i> -CL) 100/0/5	0.05	1.00	0
PLA/PCL/CNW 80/20/5	0.05	0.80	0.20
PLA/PCL/CNW-g-P(LLA- <i>co</i> -CL) 80/20/5	0.05	0.80	0.20
PLA/PCL/CNW-g-P(LLA- <i>b</i> -CL) 80/20/5	0.05	0.80	0.20

5.6 Product characterization.

The synthesized compounds were characterized using different laboratory techniques.

- Nuclear magnetic resonance ($^1\text{H-NMR}$)

The $^1\text{H-NMR}$ spectra were recorded in CDCl_3 using a spectrometer Varian “Mercury 400” operating at 400 MHz. Chemical shift (δ) for ^1H are given in ppm relative to the known signal of the internal reference (TMS).

- Attenuated total reflection infrared spectroscopy (ATR-IR)

ATR-IR spectroscopy was used to characterize the grafted polymer.

The infrared spectra were recorded using ALPHA FT-IR Spectrometers of Bruker.

- TGA analysis

The weight percentage of grafted copolymers and blends as a function of temperature was determined using a thermobalance TA Instruments, model Q500, consisting in an electronic balance placed inside an oven. The computer is connected to a system controlling the temperature of the oven, and the changes are recorded and compared to the sample's change of weight. For every analysis about 5-10 mg for each sample were weighed.

Measurements were conducted under nitrogen atmosphere from 40°C to 600°C using a heating rate modulated by the first derivative of the loss in mass.

- DSC analysis

For the thermal characterization of the copolymers and blends a differential scanning calorimeter PerkinElmer DSC 8500 has been used, equipped with a cooling system INTRACooler II with a nitrogen flow of 20 ml/min. Heating scans were performed in an inert atmosphere using high purity nitrogen. The thermal and enthalpy calibration was performed with an indium sample ($T_m = 156.6^\circ\text{C}$ and $\Delta H_m = 28.71 \text{ J/g}$). About 5 mg for each sample have been weighed. Two types of analysis were performed dynamic and isothermal.

The dynamic scans of all blends, CNW, CNW-P(LLA-*co*-CL) 7 and CNW-P(LLA-*b*-CL) was performed according to the following steps:

- Heating from 25°C to 200°C at a rate of 10°C/min, keep this temperature for 3 minutes.
- Cooling from 200°C to -20°C at a rate of 10°C/min, keep this temperature for 3 minutes.
- Heating from -20°C to 200°C at a rate of 10°C/min.

The method used for isothermal crystallization of all blends was:

- Heating from 25°C to 200°C at the speed of 20°C/min, keep this temperature for 3 minutes.
- Cooling from 200 to the isothermal crystallization temperature (T_c) at a speed of 60°C/min.
- Keep at this temperature for 30 min. This time is estimated as three times the time necessary to develop 50% of the crystals.
- Heating from T_c to 200°C at a speed of 10°C/min.

18 values of T_c have been taken (respectively 140°C, 136°C, 132°C, 128°C, 125°C, 122°C, 119°C, 116°C, 114°C, 112°C, 110°C, 108°C, 105°C, 102°C, 99°C, 96°C, 93°C, 90°C) for each sample. Each sample pan was replaced after every two isothermal analyses because the samples suffered degradation when they were subjected to many scans.

Reference:

- [1] A. Casale, L'Acido Polilattico: dalla scoperta alle applicazioni attuali, Workshop tecnico-scientifico: "Opportunità applicative del PLA: Problematiche ed aspettative", Alessandria (TO), 2014
- [2] Cabedo, Lluís, et al. "Optimization of biodegradable nanocomposites based on PLA/PCL blends for food packaging applications." *Macromolecular symposia*. Vol. 233. No. 1. WILEY-VCH Verlag, 2006.
- [3] Liu G.Y., Chen C.J., Ji J., Biocompatible and biodegradable polymersomes as delivery vehicles in biomedical applications, *Soft Matter* (2012), 8, 8811.
- [4] Luckachan G.E., Pillai C.K.S., Biodegradable Polymers- A Review on Recent Trends and Emerging Perspectives, *J Polym Environ*, (2011), 19, 637–676.
- [5] Lasprilla A.J.R., Martinez G.A.R., Lunelli B.H., Jardini A.L., Filho R.M., Polylactic acid synthesis for application in biomedical devices - A review, *Biotechnology Advances* 30, (2012), 321–328., 2011.
- [6] Wahit M.U., Akos N.H., Laftah W.A., Influence of Natural Fibers on the Mechanical Properties and Biodegradation of Polylactic acid, and Polyε-caprolactone, *Composites: A Review*, *POLYMER COMPOSITES* (2012), DOI 10.1002/pc.
- [7] McLauchlin, A.R. Thomas, N., Preparation and thermal characterisation of poly(lactic acid) nanocomposites prepared from organoclays based on an amphoteric surfactant. *Polym. Degrad. Stabil.*, Vol. 94 (5) (2009), pp. 868-872.
- [8] Ogata, N., Jimenez, G., Kawai, H., Ogihara, T., "Structure and thermal/mechanical properties of poly(l-lactide)-clay blend". *J. Polym. Sci. B, Polym. Phys.*, Vol. 35 (2), (1997), pp. 389- 396.
- [9] Goffin, Anne-Lise, et al. "Polyester-grafted cellulose nanowhiskers: a new approach for tuning the microstructure of immiscible polyester blends." *ACS applied materials & interfaces* 4(7) (2012): 3364-3371.
- [10] M. Labeta W. Thielemans *Chem. Soc. Rev.* (2009) Vol. 38 3484.
- [11] Labet, Marianne, and Wim Thielemans. "*Synthesis of polycaprolactone: a review.*" *Chemical Society Reviews* Vol. 38(12) (2009): pp. 3484-3504.
- [12] Khanna, Ashok, et al. "*Molecular modeling studies of poly lactic acid initiation mechanisms.*" *Journal of Molecular Modeling* Vol.14(5) (2008): pp. 367-374.

- [13] Stridsberg, Kajsa M., Maria Ryner, and Ann-Christine Albertsson. *Controlled ring-opening polymerization: polymers with designed macromolecular architecture*. Springer Berlin Heidelberg, 2002.
- [14] Henton, David E., et al. "Polylactic acid technology." *Natural Fibers, Biopolymers, and Biocomposites*, Taylor & Francis, Boca Raton, FL (2005): 527-577.
- [15] Bonduelle, Colin, Blanca Martin-Vaca, and Didier Bourissou. "Lipase-catalyzed ring-opening polymerization of the O-carboxylic anhydride derived from lactic acid." *Biomacromolecules* 10(11) (2009): 3069-3073.
- [16] Auras, Rafael A., et al., eds. *Poly (lactic acid): synthesis, structures, properties, processing, and applications*. Vol. 10. John Wiley & Sons, 2011.
- [17] Barton, B. F., P. D. Graham, and A. J. McHugh. "Dynamics of spinodal decomposition in polymer solutions near a glass transition." *Macromolecules* 31(5) (1998): 1672-1679.
- [18] Beaucage, G., R. S. Stein, and R. Koningsveld. "Tacticity effects on polymer blend miscibility. 1. Flory-Huggins-Staverman analysis." *Macromolecules* 26(7) (1993): 1603-1608.
- [19] *Progress in Polymer Science* 23(4) (1998): 707-757.
- [20] Halldén, Åsa, Mehrnoush Jowkar Deriss, and Bengt Wesslén. "Morphology of LDPE/PA-6 blends compatibilised with poly (ethylene-graft-ethylene oxide) s." *Polymer* 42(21) (2001): 8743-8751.
- [21] Isayev, Avraam I., and Sanjay Palsule. *Encyclopedia of Polymer Blends, Volume 2: Processing*. Vol. 2. John Wiley & Sons, 2011.
- [22] Dell'Erba, Ramiro, et al. "Immiscible polymer blends of semicrystalline biocompatible components: thermal properties and phase morphology analysis of PLLA/PCL blends." *Polymer* 42(18) (2001): 7831-7840.
- [23] Moon, Robert J., et al. "Cellulose nanomaterials review: structure, properties and nanocomposites." *Chemical Society Reviews* 40(7) (2011): 3941-3994.
- [24] Lizundia, E., J. L. Vilas, and L. M. León. "Crystallization, structural relaxation and thermal degradation in Poly (l-lactide)/cellulose nanocrystal renewable nanocomposites." *Carbohydrate polymers* 123 (2015): 256-265.
- [25] Carlmark, Anna, Emma Larsson, and Eva Malmström. "Grafting of cellulose by ring-opening polymerisation—A review." *European Polymer Journal* 48(10) (2012): 1646-1659.

- [26] Angles, M. Neus, and Alain Dufresne. "Plasticized starch/tunicin whiskers nanocomposite materials. 2. Mechanical behavior." *Macromolecules* 34(9) (2001): 2921-2931.
- [27] Youssef, Lucian A. Lucia, and Orlando J. Rojas. "Cellulose nanocrystals: chemistry, self-assembly, and applications." *Chemical reviews* 110(6) (2010): 3479-3500.
- [28] Roy, Debashish, et al. "Cellulose modification by polymer grafting: a review." *Chemical Society Reviews* 38(7) (2009): 2046-2064
- [29] Ajellal, Nouredine, et al. "Metal-catalyzed immortal ring-opening polymerization of lactones, lactides and cyclic carbonates." *Dalton Transactions* 39(36) (2010): 8363-8376.
- [30] Thillaye du Boullay, Olivier, et al. "An activated equivalent of lactide toward organocatalytic ring-opening polymerization." *Journal of the American Chemical Society* 128(51) (2006): 16442-16443.
- [31] Mazarro R., Gracia I., Rodriguez J.F., Storti G., Morbidelli M., *Polym Int* (2011)
- [32] Italian Association of Science and Technology of macromolecules (AIM), Acts of the Conference-school on "*Structural polymeric materials*". Gargnano (BS) 1989
- [33] Italian Association of Science and Technology of macromolecules (AIM), Experience days on "*Thermal characterization of polymeric materials*", Gargnano (BS), 2005
- [34] Lorenzo, Arnaldo T., et al. "DSC isothermal polymer crystallization kinetics measurements and the use of the Avrami equation to fit the data: Guidelines to avoid common problems." *Polymer testing* 26(2) (2007): 222-231.
- [35] Hobbs, J. K., *Encyclopedia of Polymer Science and Technology* Vol. 9(3) Ed. John Wiley & Sons. Inc. (2004), pp. 465-497.
- [36] Ehrenstein G.W, *Polymeric Materials*, (2001), Hanser
- [37] A.J. Müller, *Structure and properties of semi-crystalline polymers*, Venezuela, Grupo de Polímeros USB, Departamento de Ciencia de los Materiales, Universidad Simón Bolívar
- [38] Okui, Norimasa, et al. "Temperature and molecular weight dependencies of polymer crystallization." *Progress in Understanding of Polymer Crystallization*. Springer Berlin Heidelberg, 2007. 391-425.
- [39] Olabis, Olagoke. *Polymer-polymer miscibility*. Elsevier, 2012.
- [40] Abe, Hideki, et al. "Morphological and rate analyses of regime transition for poly [(S)-lactide] crystal growth." *Biomacromolecules* 2(3) (2001): 1007-1014.
- [41] Gedde, W., *Polymer Physics*, Chapman & Hall, London, 1995.

- [42] Sivalingam, G., and Giridhar Madras. "Thermal degradation of binary physical mixtures and copolymers of poly (ϵ -caprolactone), poly (d, l-lactide), poly (glycolide)." *Polymer degradation and stability* Vol. 84(3) (2004): pp. 393-398.
- [43] Lönnberg, Hanna, et al. "Grafting of cellulose fibers with poly (ϵ -caprolactone) and poly (L-lactic acid) via ring-opening polymerization." *Biomacromolecules* 7(7) (2006): 2178-2185.
- [44] Grijpma, D. W., and A. J. Pennings. "Polymerization temperature effects on the properties of l-lactide and ϵ -caprolactone copolymers." *Polymer bulletin* 25(3) (1991): 335-341.
- [45] Peponi, Laura, Angel Marcos-Fernández, and José María Kenny. "Nanostructured morphology of a random P(DLLA-co-CL) copolymer." *Nanoscale research letters* 7(1) (2012): 1-7.
- [46] Wang, Jing-Liang, and Chang-Ming Dong. "Synthesis, Sequential Crystallization and Morphological Evolution of Well-Defined Star-Shaped Poly (ϵ -caprolactone)-b-poly (L-lactide) Block Copolymer." *Macromolecular Chemistry and Physics* 207(5) (2006): 554-562
- [47] Di Lorenzo, Maria Laura. "The Crystallization and Melting Processes of Poly (L-lactic acid)." *Macromolecular symposia*. Vol. 234. No. 1. WILEY-VCH Verlag, (2006): 176-183.
- [48] A. T. Lorenzo, "Avrami and LH Plugin for Origin". Available at: <https://sites.google.com/a/usb.ve/ajmuller/downloads/plugins> June 2013
- [49] Marand, Hervé, Jiannong Xu, and Srivatsan Srinivas. "Determination of the equilibrium melting temperature of polymer crystals: linear and nonlinear Hoffman-Weeks extrapolations." *Macromolecules* 31(23) (1998): 8219-8229.